N72-26239

# NASA TECHNICAL MEMORANDUM
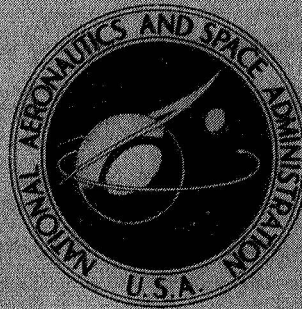
NASA TM X-2566

CASE FILE
COPY

A SURVEY OF NASA LANGLEY STUDIES
ON HIGH-SPEED TRANSITION
AND THE QUIET TUNNEL

by Ivan E. Beckwith and Mitchel H. Bertram

Langley Research Center

Hampton, Va. 23365

1. Report No. NASA TM X-2566	2. Government Accession No.	3. Recipient's Catalog No.
4. Title and Subtitle A SURVEY OF NASA LANGLEY STUDIES ON HIGH-SPEED TRANSITION AND THE QUIET TUNNEL		5. Report Date July 1972
		6. Performing Organization Code
7. Author(s) Ivan E. Beckwith and Mitchel H. Bertram		8. Performing Organization Report No. L-8311
9. Performing Organization Name and Address NASA Langley Research Center Hampton, Va. 23365		10. Work Unit No. 136-13-04-01.
		11. Contract or Grant No.
12. Sponsoring Agency Name and Address National Aeronautics and Space Administration Washington, D.C. 20546		13. Type of Report and Period Covered Technical Memorandum
		14. Sponsoring Agency Code

15. Supplementary Notes   The present paper is based on a paper presented at the 1971 Boundary Layer Transition Specialists Workshop in San Bernardino, California, Nov. 3-5, 1971, in two parts as "Effects of Wind-Tunnel Disturbances on Hypersonic Transition and Basic Concepts for Quiet Tunnel Development" by Mitchel H. Bertram and "Review and New Results for Correlations of Transition Data on Cones and Space Shuttle Configurations" by Ivan E. Beckwith.

16. Abstract

The present studies include a quantitative experimental and theoretical assessment of the role of wind-tunnel disturbances in the boundary-layer transition process at hypersonic speeds. The various approaches and recent results for the development of a low-noise-level tunnel are presented. A statistical parametric study of transition data with a large computer is shown for cones in free flight, ballistic ranges, and wind tunnels at essentially zero angle of attack. New transition results for slender cones at small angle of attack are also given, as are studies of transition at high angle of attack, which are compared with various correlation attempts. Included are results which indicate that hypersonic transition in the outer part of the boundary layer precedes the manifestation of transition at the wall ("precursor" transition).

17. Key Words (Suggested by Author(s)) Boundary layer Transitional boundary layer Shear layers		18. Distribution Statement Unclassified — Unlimited	
19. Security Classif. (of this report) Unclassified	20. Security Classif. (of this page) Unclassified	21. No. of Pages 67	22. Price* $3.00

CONTENTS

A SURVEY OF NASA LANGLEY STUDIES ON HIGH-SPEED
TRANSITION AND THE QUIET TUNNEL*

By Ivan E. Beckwith and Mitchel H. Bertram
Langley Research Center

SUMMARY

This paper reviews current research on boundary-layer transition and related aspects of other studies at the NASA Langley Research Center. These studies include a quantitative experimental and theoretical assessment of the role of wind-tunnel disturbances in the transition process at hypersonic speeds. The results show that at a given local Mach number, a unique relationship exists between root-mean-square sound pressure and transition Reynolds number on sharp cones and reemphasize the urgent requirement for a quiet supersonic tunnel. The various approaches and recent results for the development of a low-noise-level tunnel are presented. Shown also are preliminary computations from a linear stability analysis of two-dimensional supersonic flows in a channel.

Achievement of the prediction of boundary-layer transition from first principles still lies in the future. Thus, the design engineer relies on experience and uses transition data correlations based on parameters that presumably produce minimum deviations from mean curve fits. Such a statistical parametric study of transition data with a large computer is presented for cones in free flight, ballistic ranges, and wind tunnels at essentially zero angle of attack. New results for cones at small angle of attack are also given. Space shuttle vehicles, however, generally operate at moderate to high angles of attack, and transition location can have a large impact on the design of thermal protection systems. Thus, the results of studies at Langley on transition at high angles of attack are presented and compared with various correlation attempts. Also, recent transition results from free shear layers are compared with previous results from shear layers over separated regions in supersonic flow.

---

*The present paper is based on a paper presented at the 1971 Boundary Layer Transition Specialists Workshop in San Bernardino, California, Nov. 3-5, 1971, in two parts as "Effects of Wind-Tunnel Disturbances on Hypersonic Transition and Basic Concepts for Quiet Tunnel Development" by Mitchel H. Bertram and "Review and New Results for Correlations of Transition Data on Cones and Space Shuttle Configurations" by Ivan E. Beckwith.

INTRODUCTION

Accurate predictions for the location of transition and the streamwise extent of transitional flow are required in order to reduce the design uncertainties of vehicle components such as inlets, control surfaces, and leading-edge regions. Accurate predictions for the entire aircraft become critical for hypersonic vehicles since, for some operational conditions, the boundary layers on appreciable portions of these vehicles may remain laminar or transitional. Significant increases in range and performance and reduced requirements for heat-protection systems are then possible. As an example, space-shuttle studies have indicated that turbulent heating can have a large impact on the design of thermal protection systems, both in choice of heat-shield materials and in system unit weight. (See ref. 1.) The extent of turbulent heating depends on transition location, and these studies show the need for additional work to define more clearly the proper criteria to be used for boundary-layer transition.

Some available transition results indicate that the area affected by boundary-layer transition (and thus turbulent heating) varies roughly as the square of the distance from the trailing edge. Thus, transition far forward on the vehicle can affect large areas, but if transition occurs reasonably far back, only a relatively small area will be affected. Since thermal protection system weights vary from 48 N/m^2 (1 lb/ft^2) at an exterior wall temperature of 810 K (1000° F) to over 96 N/m^2 (2 lb/ft^2) at 1370 K (2000° F), increased confidence in data for higher transition Reynolds numbers could lead to major weight savings as well as improved reuse capabilities, ease of manufacturing, and lower cost. Thus, the ability to predict the correct transition Reynolds numbers is of increasing importance. Similar arguments can be advanced for other types of vehicles which operate in entirely different modes. For instance, Martellucci (ref. 2) states that the angle-of-attack divergence normally encountered in the transitional boundary-layer altitude regime by slender reentry vehicles can be attributed in whole or in part to the forces and moments due to asymmetrical transition.

Another design problem involves the structural response to the intensity and frequency of fluctuating pressure loads in transitional flow regions. Little knowledge exists concerning the frequency range of such loads under supersonic flight conditions, since the location and behavior of transitional flow cannot yet be duplicated in ground facilities and noise from the tunnel walls causes spurious indications by sensors in a model. It has been known for many years that the intensity of fluctuating pressure loads increases sharply in transitional flow regions. Again, if transitional flow occurs over large portions of a vehicle, these problems become critical.

The 1967 Boundary Layer Transition Study Group Meeting highlighted the predominant role of noise radiated from the turbulent boundary layer on hypersonic nozzle walls in boundary-layer transition on models. (See refs. 3 and 4.) In the spirit of these

2

revelations and with the continued work on concepts for a quiet tunnel and correlations of transition data at the NASA Langley Research Center (ref. 4), the most recent findings in these areas are presented.

SYMBOLS

Values are given in both SI and U.S. Customary Units. The measurements and calculations were made in U.S. Customary Units.

A,B coefficients of linear curve fit (see eq. (6) and table II(b))

a speed of sound

a^* critical velocity at minimum of gap between rods, v_{gap}

a_{ij} coefficients in F_2 correlation parameter (see eq. (5))

b_i function of M_e defined by equation (8)

c_p specific heat at constant pressure

D base diameter of cone

D^* test-section diameter or height of wind tunnel

d rod diameter

e hot-wire output

F_1,F_2 functions of M_e and $\dfrac{h_w}{h_e}$ (see eq. (5))

f frequency, hertz

h static enthalpy

$\bar{h}$ heat-transfer coefficient

K parameter relating u' and p' (see eq. (1))

l distance from start of free shear layer to transition (see fig. 24)

M   Mach number

$\dot{m}$ mass flow rate

n   exponent in transition parameters (see eqs. (4))

p   pressure

p'   root-mean-square fluctuating pressure

q   dynamic pressure, $\frac{1}{2}\rho u^2$

R   local unit Reynolds number, $\dfrac{\rho_e u_e}{\mu_e}$

R_D local Reynolds number based on D, $\dfrac{\rho_e u_e D}{\mu_e}$

R_x local Reynolds number based on x, $\dfrac{\rho_e u_e x}{\mu_e}$

R_{δ^*} local Reynolds number based on δ^*, $\dfrac{\rho_e u_e \delta^*}{\mu_e}$

$R_{\infty,r}$ free-stream Reynolds number based on nose-tip radius, $\dfrac{\rho_\infty u_\infty r}{\mu_\infty}$

r   nose radius of cones

s   distance from cone tip to pressure transducer (see fig. 1)

T   absolute temperature

u   velocity in x-direction

u'   root-mean-square fluctuating velocity

v   velocity normal to rod axes

W   channel width

4

w	gap between rods
x	distance from leading edge
y	distance normal to surface
α	angle of attack
α_w	local angle of attack of windward line of symmetry
α_δ	dimensionless wave number, $\dfrac{2\pi\delta}{\lambda}$
γ	ratio of specific heats
δ	boundary-layer thickness
δ_e	arc tan $\dfrac{v_e}{u_e}$

$\delta_{eff} = \alpha - \delta_e$

δ^*	local-similarity displacement thickness (see ref. 4)
θ	momentum thickness of boundary layer
θ_c	cone half-angle
θ_w	shock-wave angle
λ	disturbance wavelength
μ	viscosity
ρ	density
ρ^*	density at minimum gap between rods
σ_x	deviation, in terms of x-location of transition, from least-squares curve fit of data

Subscripts:

e   local free stream

o   zero gap opening or tunnel stagnation conditions

t   beginning of transition

w   wall

∞ free stream ahead of bow shock

2   reference conditions for free shear layer (see fig. 24)

WIND-TUNNEL DISTURBANCE EFFECTS ON TRANSITION

Experimental Studies

This section reports on two studies of facility disturbance effects on transition with different approaches to the measurement of the disturbance environment. In one study, conducted in several wind tunnels, dynamic-pressure transducers mounted flush with the model surface gave the level of sound disturbances beneath the laminar boundary layer. In the second study, a constant-current hot-wire anemometer measured free-stream and local inviscid flow-field disturbances in two hypersonic helium wind tunnels. The first approach has the advantage of requiring relatively simple instrumentation. The second approach, the hot-wire technique, gives detailed information concerning the actual disturbances imposed on the boundary layer.

In the first study (refs. 5 and 6), laminar-boundary-layer transition locations and fluctuating pressure levels and spectra were measured on two sets of sharp cones in several hypersonic facilities at the Langley Research Center. One set of cones was instrumented with thermocouples and one set with dynamic-pressure transducers. The pressure transducers were mounted flush with the surface of the cones and were generally under the laminar portion of the boundary layer. The cone semiapex angles were selected to give a local Mach number of 5 for these tests. Therefore, except for variations in total temperature and wall-to-total temperature ratio, which are believed to have a minor influence, the laminar-boundary-layer profile shapes on the various conical models were nearly the same. This experimental approach resembles the method of stability analysis in that the response of a (presumed) fixed laminar profile subjected to different disturbances is observed.

6

A list of the test conditions for the facilities and the cone half-angles θ_c used in the first experiment is presented in table I. The cross-sectional sketch of the pressure model given in figure 1 illustrates the dominant wind-tunnel disturbances that originate from the tunnel turbulent boundary layers for $M_\infty > 3$. (See refs. 7 to 13.)

In the second study (refs. 5 and 14), the influence of tunnel disturbance level on boundary-layer transition on a 2.87° half-angle cone was examined in two hypersonic helium tunnels with unheated flow. Thermocouples gave the surface heating rates, and free-stream and shock-layer disturbance levels were obtained with a constant-current hot-wire anemometer. The nominal Mach numbers in the two helium facilities were 18 and 20, which produced edge Mach numbers of about 14 and 16, respectively.

The facilities were the Langley 22-inch helium tunnel ($M \approx 20$) and the 150-cm (60-in.) leg ($M \approx 18$) of the Langley Mach 20 high Reynolds number helium tunnel. Local Reynolds numbers based on the 150-cm (60-in.) model length varied from 30×10^6 to 87×10^6. The wall temperature about equaled the total temperature.

Spectra of the hot-wire signals in the free stream and the shock layer from tests in the 150-cm (60-in.) helium tunnel are shown in figure 2(a). The spectra in the free stream are typical of the wide-band sound radiated from turbulent boundary layers with most of the energy occurring at frequencies associated with scales and velocities of large dominant disturbances. In the shock layer some redistribution of the spectra seems to occur, especially at the highest stagnation pressure. Another interesting feature is the gradual development of a discrete component in the spectra at approximately 70 kHz, believed to be associated with boundary-layer transition. Spark schlieren of the flow at 1100 N/cm^2 (1600 psi) tunnel stagnation pressure indicates that transition begins about 50 cm (20 in.) from the cone tip near the outer edge of the boundary layer. Surface heat-transfer measurements show transition at 84 cm (33 in.) from the cone tip. The hot wire was 89 cm (35 in.) from the tip. (This "precursor" transition phenomenon will be discussed in more detail later in this paper.) Early in transition the schlieren shows disturbances with scales on the order of twice the boundary-layer thickness, about 1.27 cm (0.50 in.). If the disturbance velocity was assumed to be equal to the cone shock-layer velocity, the corresponding frequency would be about 70 kHz. Therefore, the transition process on the cone appears to display some frequency selectivity. The redistribution of the spectra at the highest stagnation pressure may also be associated with "precursor" transition in the cone boundary layer.

Spectral distributions obtained from the surface pressure transducers on a cone in two air facilities (Langley Mach 8 variable-density hypersonic tunnel and the Langley 20-inch Mach 6 tunnel) are shown in figure 2(b). The average of these distributions is the root mean square (rms) of the fluctuating pressure over the frequency range shown. The ordinate scale represents the level of fluctuating pressure as a function of frequency

recorded in bandwidth increments of 1.6 kHz. Both spectra are broadband with most of the energy in the low-frequency ranges again associated with the scales and velocities of dominant disturbances in the tunnel-wall turbulent boundary layer. One interesting result can be noted from the spectra, namely, the unexpected disturbances at approximately 45 kHz. The origin of these disturbances is not known, but they could be due to some flow phenomenon or may be associated with the pressure pickup and its response to fluctuating pressures in the neighborhood of 45 kHz.

Since the pressure fluctuation levels in the surface pressure study were measured under the laminar portion of the boundary layer on cones, the relation of these levels to those in the free stream must be determined. In figure 3 the pressure fluctuation levels obtained by Stainback (ref. 5) are compared with the hot-wire data reported by Laufer (ref. 10). (Here it was assumed that the appropriate correlating parameters for p'/p_e are free-stream Mach number and free-stream Reynolds number based on tunnel diameter.) Although some scatter exists in both Laufer's data and the present results, reasonable agreement occurs between the two sets of data. Note, however, that the average level of the surface pressure data is 15 to 20 percent below the free-stream hot-wire data at $R_{\infty,D^*} \approx 7 \times 10^6$.

The basic data for transition location obtained in the two studies are shown in figure 4(a) as a function of local unit Reynolds number. These results illustrate the different levels of the transition Reynolds numbers between the two studies and also within the first study where $M_e = 5$ with essentially identical laminar boundary layers on the models. These latter results indicate that some facility characteristic has a strong influence on transition Reynolds number.

The fluctuating-pressure-level data are presented in figure 4(b) in terms of the rms fluctuating pressure normalized by the local static pressure plotted against the local unit Reynolds number. The rapid increase and peak in the fluctuating pressure level measured on the model in the Mach 6 high Reynolds number tunnel for $R = 6 \times 10^7$ to 8×10^7 per meter $(2 \times 10^7$ to 2.5×10^7 per foot) result from the movement of transition upstream of the pressure pickup which was located 10 cm (4 in.) from the apex of the model (fig. 1). The measurements of the free-stream disturbances (predominantly sound radiated from the nozzle-wall turbulent boundary layer) with the hot-wire anemometer indicate a nearly constant disturbance level over the operating range of the larger Mach 18 facility, whereas the disturbance level decreased substantially with unit Reynolds number (above $R = 10 \times 10^6$ per meter $(3 \times 10^6$ per foot) where the nozzle boundary layer is turbulent) in the 22-inch helium tunnel $(M \approx 20)$. The disturbance levels were obtained from mode diagrams. (See ref. 15.) Hot-wire measurements were obtained in the 150-cm (60-in.) facility in both the free stream and the 2.87° cone shock layer. These measurements (fig. 4(b)) indicate: (1) The disturbance levels in percent of local mean quantities remain approximately constant across the shock, and (2) no significant distur-

bance levels of the other modes (vorticity or entropy) are produced when the free-stream sound disturbances are processed by the shock. These conclusions only apply for the weak hypersonic shock on the 2.87^o cone.

Comparison of the hot-wire results from tests in the shock layer of the 16° cone in the 22-inch helium tunnel with data in the free stream (fig. 4(b)) indicates that the stronger shock causes about a 25-percent reduction in p'/p_e at $R \approx 10 \times 10^6$ per meter (3×10^6 per foot). The surface pressure measurements on this cone again agree with the hot-wire data in the cone shock layer. The reduction in the free-stream level of p'/p_e across the cone shock is consistent with the comparison of figure 3, where cone surface pressure levels were also smaller than free-stream values at $R_{\infty,D*} \approx 7 \times 10^6$. Additional hot-wire data illustrating the effects of shock strength on rms disturbance levels are given in reference 5.

Transition Reynolds numbers measured in the two helium tunnels on the 2.87^o cone were found to display a "unit Reynolds number" effect, but to different degrees. (See fig. 4(a).) This result is consistent with the hot-wire measurements (fig. 4(b)) and indicates again that the model transition processes are dominated by the disturbances radiated by the tunnel-wall turbulent boundary layers.

In figure 5 the transition Reynolds numbers of figure 4(a) are plotted as a function of the fluctuating-pressure-level data of figure 4(b). (Data from the Mach 6 high Reynolds number tunnel for $R > 6 \times 10^7$ per meter (2×10^7 per foot) have been excluded.) This figure shows that at $M_e = 5$ a unique relationship exists for air boundary layers between transition Reynolds numbers and the normalized rms pressure fluctuations measured beneath the laminar portion of the boundary layer. The transition Reynolds numbers vary almost inversely with the fluctuating pressure levels. Since the laminar-boundary-layer profiles were maintained nearly invariant in the first study, this result shows that the sound level dominates wind-tunnel transition.

The data from the second study represent the first combined transition and hot-wire investigation above $M_e = 6.7$ and indicate that the tunnel disturbance level has a strong influence on cone boundary-layer transition up to at least $M_e = 16.2$. Also, comparison of cone transition data obtained in the two hypersonic helium tunnels at the same noise level suggests that transition Reynolds number is not a strong function of local Mach number for $M_e \geqq 14$.

The conclusions of references 7 and 12 were that the transition Reynolds numbers depended mainly on parameters which control the pressure fluctuation level in the test section (that is, test-section circumference and properties of the tunnel-wall turbulent boundary layer, such as displacement thickness and mean skin-friction coefficient) and were independent of local Mach number. The present results combined with previously published results (refs. 8 and 16 to 18) shown in figure 5 suggest that transition Reynolds

number is also a function of parameters governing the characteristics of the laminar profile — that is, Mach number, total temperature, wall-to-total temperature ratio, and test gas. Thus, transition measured on cones in wind tunnels cannot be expected to correlate solely in terms of local or free-stream parameters but by a combination of these parameters. The results in figure 5 also show that nearly the same inverse relation between the transition Reynolds number and the disturbance level was observed in several air and helium facilities over a wide Mach number range. Therefore, in accordance with previous results, the rms level of the sound radiated from the tunnel-wall turbulent boundary layer dominates the transition process. It follows that the application of wind-tunnel transition data to the prediction of transition in flight cannot be relied upon without some knowledge of corresponding disturbance levels in flight. The need for a "quiet" wind tunnel with reduced and/or controlled levels of sound radiation (by maintaining laminar boundary layers on the tunnel walls, for example) for transition research is evident and will be discussed later in this paper.

Theoretical Studies

Correlations of transition data in terms of gross flow properties associated with the boundary layer and in terms of environmental disturbances are at present the only sources of information available for predicting the location and extent of transition. Meanwhile, theoretical methods based on numerical solution techniques are being developed. Preliminary results obtained from one of these theoretical studies (under NASA Contract No. NAS1-10865 by United Aircraft Research Laboratory (UARL)) are presented in figures 6 and 7. This procedure, developed by McDonald and Fish (ref. 19), utilizes an independent equation that governs the production, convection, and decay in kinetic energy of the disturbances in a transitional flow. The only inputs required in the procedure are the usual boundary conditions plus the measured free-stream rms sound levels, which are related to the kinetic energy of the disturbances through plane acoustic wave approximations and an arbitrary constant K. At this stage in the development of the theory, the arbitrary constant K determines the general location of transition (one measured location for transition and noise-level measurements are sufficient). The transition data in figure 6 are from the tests in the Mach 6 and 8 air wind tunnels (figs. 4 and 5). These results show a prediction of the correct trend of transition with changes in rms sound level. The heat-transfer data in figure 7 are typical results obtained during this same study and show that the extent of transitional flow is predicted with mixed success by this procedure.

Since the UARL procedure utilizes the rms free-stream fluctuating velocities rather than free-stream fluctuating pressures, they assumed that the velocity and pressure fluctuations can be related by an expression of the type

$$\frac{u'}{u_e} = \left(\frac{K}{\gamma M_e}\right)\left(\frac{p'}{p_e}\right) \qquad (1)$$

based upon the unsteady propagation of a plane-wave disturbance. The use of the UARL finite-difference procedure (ref. 19) for "predicting" transition and the use of equation (1) to relate velocity and pressure fluctuations obviously represent great oversimplifications of the physical processes involved. Hence, while the values of K required in the UARL calculations to match the transition data (fig. 6) may depend on M_e and on some wave propagation properties, other factors not accounted for in this simple theory may also affect the required values of K.[1]

LAMINAR FLOW CONTROL AND THE QUIET TUNNEL

Laminarization Through the Use of Suction

The results from a cone model tested by Morrisette in the Mach 4 area suction nozzle described in reference 4 were disappointing. The transition Reynolds numbers were no better, in fact slightly worse, than those measured in the equivalent solid nozzle. This behavior is ascribed to the small scale of the test apparatus and the correspondingly large nozzle porosity which introduced noise into the model environment through roughness and hole suction effects.

With scale an important parameter, another route has been taken to evaluate the continuous surface porosity approach. This porous surface effort will be continued, but in cooperation with Klebanoff and Spangenberg at the National Bureau of Standards (NBS). They have shown considerable success in their own nozzle laminarization work utilizing longitudinal suction slots at a Mach number of 2, as illustrated in figure 8. A. L. Nagel at Langley supervised the construction of a porous wall, to fit this NBS nozzle, using finer mesh material than in our unsuccessful tests. This new material, together with the larger size of their nozzle, should enable a more critical test of the validity of the area suction approach.[2]

---

[1]More recent results under this contract redefine K so that the factor $K/\gamma M_e$ in equation (1) is replaced by $K/\gamma M_e M_r$, where M_r is the Mach number of the pressure wave relative to the free stream as given by Laufer. A determination of this new K gives a value of 1.45 for all three sets of data.

[2]Some of these experiments have since been carried out by Klebanoff and Spangenberg. Laminar flow was maintained past the last measuring station on the porous wall (26.7 cm (10.5 in.) from the throat) at a unit Reynolds number of about 12×10^6 per meter (3.5×10^6 per foot). Transition moved rapidly forward with increasing unit Reynolds number, with only 10 cm (4 in.) of laminar flow at $R = 14 \times 10^6$ per meter (4.3×10^6 per foot). This behavior is characteristic of three-dimensional roughness tripping. Klebanoff and Spangenberg also detected a pattern of disturbances emanating from the porous surface. These disturbances were primarily due to nonuniform suction, rather than surface irregularities, and were several times stronger when suction was applied than without suction.

With the use of lateral suction slots, Groth obtained laminar flow for length Reynolds numbers up to 7×10^6 on a body of revolution at a Mach number of 3.0. (See ref. 20.) In more recent experiments, laminar flow was observed at much larger Reynolds numbers for similar test conditions. However, Groth found that lateral slots in supersonic flow introduce substantial disturbances into the free stream. The NBS group recently obtained laminar flow at length Reynolds numbers to about 3.3×10^6 by the use of longitudinal suction slots on the sidewall of their nozzle. (See fig. 8(c).) This concept of utilizing boundary-layer removal through slots between longitudinal rods for laminar boundary-layer control is also under study at Langley with preliminary tests utilizing the model shown in figure 9. This model consists of 35 rods of 0.64-cm (0.25-in.) diameter mounted on three crossmembers. The gaps between the rods can be adjusted from closed to any desired opening. The forward crossmember consists of a sharp flat plate with a 15° beveled section which supports the rods as shown in the inset sketch of figure 9. The total length of the model was 47.8 cm (18.8 in.). Two of the 35 rods were hollow tubes of 0.76-mm (0.030-in.) wall thickness. The phase-change paint technique (ref. 21) was used to obtain indications of transition location and heating rates on the hollow tubes.

The model was tested in the Langley Mach 8 variable-density hypersonic tunnel. In order to obtain sufficient suction for partial boundary-layer removal through the gaps, the model was oriented so that the surface of the model shown in figure 9 faced windward at 5° and 10° angle of attack to provide sufficient pressure drop across the model for sonic cross flow through the gaps.[3]

The effect of the suction reduces the height of the inviscid flow field slightly and decreases the boundary-layer thickness considerably. This effect has been determined from schlieren photographs such as figure 10, which shows the rod suction model at $\alpha = 5^\circ$ with the gaps closed (fig. 10(a)) and the gaps open to 1.27 mm (0.050 in.) (fig. 10(b)). The short wedge model above and to the right of the rod model housed a flush-mounted dynamic-pressure transducer which measured the sound within the flow field of the rod model. The results of these sound measurements are presented later. First, the effects of suction on the inviscid and boundary-layer flow will be presented.

A comparison has been made between the variation in measured shock-wave angle with gap opening and stagnation pressure and the results of a simple inviscid calculation. This inviscid calculation uses the assumption of inviscid sonic flow through the gap openings normal to the rod axes. Hence, the formula for the mass flow ratio is

---

[3]More recent pressure measurements on the same model by William D. Harvey at Langley indicate that at $\alpha = 5^\circ$ sonic cross flow through the gaps did not occur on the aft portion of the model, whereas at $\alpha = 10^\circ$ sonic flow occurred over the entire model for all gap settings.

$$\frac{\dot{m}}{\dot{m}_e} = \frac{\dfrac{\rho^*}{\rho_e}\dfrac{a^*}{a_e}\,w}{M_e(w+d)} \tag{2}$$

which is plotted against gap opening on the right-hand side of figure 11, where

$$\frac{\left(\rho_w v_w\right)_{mean}}{\left(\rho u\right)_e} = \frac{\dot{m}}{\dot{m}_e} \quad \text{and} \quad \left(\rho_w v_w\right)_{mean} \text{ is the mean suction mass flow through the model}$$

per unit area of model surface. The effective deflection angle for the inviscid flow is

$$\delta_{eff} = \alpha - \delta_e \tag{3}$$

where

$$\tan \delta_e = \frac{v_e}{u_e}$$

The following sketch illustrates the notation:
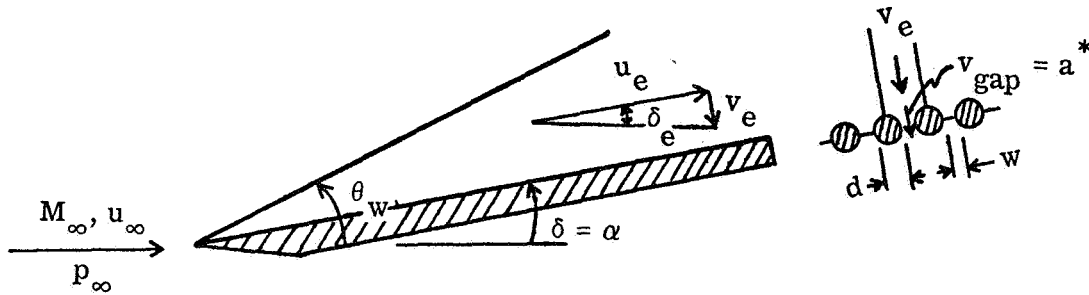
The shock-wave angle is then calculated for the effective deflection angle δ_{eff}. The mea-sured values of θ_w show some scatter; however, the agreement with the theory in fig-ure 11 indicates that the assumption of inviscid sonic cross flow through the gaps is reasonable.

The suction mass flow rates from equation (2) have been used in the finite-difference theory of Harris (ref. 22) as distributed area suction rates, and resulting values of boundary-layer thickness and heat transfer (for laminar flow) are compared with experi-mental values in figures 12(a) and 12(b), respectively. Since the measured values of boundary-layer thickness were obtained directly from schlieren photographs, accurate values were not expected. Nevertheless, trends from the experimental data are in rea-sonable agreement with trends of the calculated values. However, the disagreement in trends and magnitudes between predicted ratios of heat-transfer coefficient and experi-

mental values (fig. 12(b)) indicates that the flat-plate area suction analysis may not be valid or that the reference heating values (for zero gap opening) were turbulent. These reference values were obtained at the downstream side of the uncertainty band for transition on the model with gaps closed (fig. 13).[4]

The locations of transition on the rod model are shown as a function of tunnel stagnation pressure in figure 13 for closed gaps and three different gap openings at $\alpha = 10^O$ and for 1.27-mm (0.050-in.) gaps at $\alpha = 5^O$. Also shown in the figure for comparison are the transition locations on a flat plate at $\alpha \approx 5^O$ and 10°. The locations of transition on the model with the gaps closed are approximately the same as on the flat plate. However, suction generally delayed transition which apparently moved off the end of the model at the lower tunnel pressures and larger gap openings. The maximum length transition Reynolds number obtained in these preliminary tests was 12×10^6 at $\alpha = 10^O$ with the gap openings set at 1.27 mm (0.050 in.). This transition Reynolds number corresponds to the point in figure 13 for $p_O = 1050$ N/cm^2 (1515 psia) at $x_t = 0.27$ meter (0.9 ft) where disturbances from the center support probably caused transition.

Fluctuating pressures were measured within the flow field of the rod suction model with flush-mounted pressure transducers located 7.6 cm (3 in.) from the leading edge on the surface of a 15-cm by 15-cm (6-in. by 6-in.) flat plate. This flat-plate model was then mounted with its surface parallel to and 1.5 cm (0.6 in.) from the windward side of the rod model, as indicated in figure 10. The results of the sound measurements are shown in figure 14, where rms p'/p_e is plotted against tunnel stagnation pressure. With the gaps set at 1.27 mm (0.050 in.), suction reduces the rms sound levels by 20 to 30 percent below the corresponding flat-plate values. These latter values were the same as the values with the gaps closed on the rod model except for $p_O \gtreqless 700$ N/cm^2 (1000 psia). At this pressure, transition on the rod model with gaps closed occurred at $x_t \approx 0.09$ meter (0.3 ft) (fig. 13) or 0.15 meter (0.5 ft) ahead of the pressure-gage location which is then well within the zone of radiated noise from the turbulent boundary layer on the rod model.

---

[4]More recent heat-transfer data obtained by William D. Harvey from thermocouples installed in the two hollow tubes indicate that $\bar{h}/\bar{h}_O$ increases from about 1.2 at $w = 0.25$ mm (0.01 in.) to a maximum of 3.0 at $w = 1.3$ mm (0.05 in.). The original values shown in figure 12(b) where $\dfrac{\bar{h}}{\bar{h}_O} < 1.0$ are now believed to be in error because of faulty test procedures, which have since been corrected. On the basis of the physical phenomenon involved, the heat transfer should always increase when the gaps are opened (provided the boundary layer is laminar for gaps closed and open) because of the reduced boundary-layer thickness.

Further reductions in noise may be possible by cleaning up the present rod model and by improving the model in the region of expansion from the leading-edge flat-plate section to the rod section.[5]

The Need for a Quiet Tunnel

Recent research at the Langley Research Center, as reported above, and previous work elsewhere have shown that transition in wind tunnels at Mach numbers greater than 3 is dominated by acoustic disturbances generated by the turbulent boundary layers on the tunnel sidewalls. Previous attempts to determine the effects on transition of flow parameters such as Mach number, wall temperature, pressure gradient, and angle of attack are therefore of questionable validity since transition is a nonlinear phenomenon. Thus, the levels and probably the trends of transition Reynolds numbers measured in wind-tunnel tests cannot be considered reliable indicators for flight conditions except when other factors such as strong cross flows or roughness dominate the transition process. Hence, in order to conduct valid wind-tunnel studies of transition, including the streamwise extent of transitional flow, one must either remove the turbulent sidewall boundary layers with scoops or ducts, shield the test models from the radiated sound, or maintain laminar sidewall boundary layers with laminar-flow-control techniques. Research to determine which of these approaches or combinations of these approaches is the most feasible and has the highest probability of success is now underway at Langley and NBS.

Application of the rod suction concept to the construction of a slotted shield, the use of subsonic lateral slots, and the use of a rapid expansion nozzle to help maintain laminar flow in the test section are illustrated in figure 15. On the basis of results of the NBS tests and the rod suction model tests presented previously, the use of these concepts should significantly reduce the levels of radiated sound within the test region of a hypersonic wind tunnel.

Stability of High-Speed Channel Flow

The work of Leach at Virginia Polytechnic Institute and State University, under NASA grant NGR 47-004-089, indicates that one need not have a turbulent boundary layer on a channel wall to alter the stability of another boundary layer in its proximity. He finds that to analyze the stability of supersonic channel flows, one must account for the fact that disturbances which originate in the boundary layer on one wall propagate across

---

[5]More recent noise data obtained at $\alpha = 10^\circ$ by P. Calvin Stainback at Langley indicate a reduction in rms noise level of about 40 percent for all gap openings from 0.25 mm (0.01 in.) to 1.27 mm (0.050 in.). This improvement in noise reduction over that noted herein for $\alpha = 5^\circ$ is believed to be due to the presence of sonic gap flow over the entire model at $\alpha = 10^\circ$.

the channel and interact with the flow on the opposite wall. In the linear analysis employed by Leach, disturbances from the boundary layer on one surface interact only with small flow disturbances of the same frequency and wavelength in the boundary layer on the other surface. Further simplifications are imposed by restricting the problem to that of determining the stability of the developing flow between two semi-infinite flat surfaces oriented parallel to the main flow stream. While the results presented herein are for equal boundary-layer thicknesses on the two plates, results have also been obtained for unequal boundary-layer thicknesses.

In order to solve the small perturbation equations to determine the interaction between the boundary layers at the two channel walls, Leach employs a procedure developed by Mack (ref. 23) for a flat plate in an infinite flow field. First, the equations for small disturbances are solved in the free stream between the two boundary layers. In this problem, an analytical solution, which consists of six independent functions, is obtained. Three of the six functions decrease exponentially away from one of the surfaces and represent disturbances which originate or reflect from the boundary layer at that surface. The other three functions decrease exponentially from the opposite wall and represent disturbances leaving the boundary layer on that wall. After the free-stream solution has been obtained, the governing equations for the flow inside the two boundary layers are solved numerically. Six independent solutions are obtained by numerically integrating from the outside edge of the boundary layer (where the numerical solution is equated to one of the analytic functions) inward to the wall. The integration is performed for each of the six functions obtained in the free-stream solution. The six independent functions obtained by solving the governing equations can be combined to form a nontrivial solution giving the propagation and growth rates of small disturbances. The curve of neutral Reynolds number at which the growth rate is zero divides the wave-number—Reynolds-number plane into a stable and unstable region.

With equal channel-wall boundary-layer thicknesses, two separate neutral Reynolds number curves may be calculated for each value of the channel width, one of which is higher than the corresponding isolated flatplate value and one lower, as shown in figure 16. An examination of the perturbation variables computed for the two neutral Reynolds number curves shows that a symmetrical perturbation flow field corresponds to the curve with the largest neutral Reynolds numbers, whereas an antisymmetrical perturbation flow field corresponds to the curve of lowest neutral Reynolds numbers. The smaller critical Reynolds number computed for the antisymmetrical perturbation field would govern the stability of the prescribed flow. For large channel widths (W large), flow perturbations originating in the boundary layer on one of the channel walls are damped by the viscosity of the fluid between the channel-wall boundary layers to such an extent that they have little effect on the stability of the flow on the opposite wall. For example, the curve labeled W = 24 to ∞ in figure 16 represents the neutral Reynolds number variation calculated for

W = 24 and W = ∞ which indicates little effect of tunnel width for values of W greater than 24 for cases with equal channel-wall boundary-layer thicknesses.

CORRELATIONS OF TRANSITION DATA

The brief review in this report has shown that since the 1967 conference on transition, some progress has been achieved in understanding transition on simple bodies in wind tunnels and in the possibility of reducing or controlling wind-tunnel disturbances.

A large amount of new flight data has been accumulated since the 1967 conference. Some of these data were obtained under rigidly controlled and accurately measured conditions (for example, the Reentry F flight, refs. 24 and 25). Several groups have completed detailed studies of these flight data and have obtained excellent correlations of selected data from single classes of vehicles.

Thus, transition research increases the capability to predict the effective location of transition and at least the mean flow properties of the boundary layer in the transitional region. Achievement of the goal of prediction from first principles still lies far in the future. Meanwhile, the design engineer necessarily relies on previous experience in the form of whatever incomplete and sometimes conflicting data he can find. The time-honored approach attempts correlations of transition Reynolds numbers with the most favored and useful parameters that are recorded in the literature on experimental studies.

Correlations for Sharp Cones at $\alpha \approx 0^{\circ}$

Since the complete test environment is seldom measured and reported, the results of such correlation attempts cannot be expected to reduce the uncertainty bounds below some limit. This limit for sharp cones at small angle of attack can be determined with considerable confidence because of the large amount of data now available from wind-tunnel, ballistic-range, and free-flight tests. Limited results of a statistical, parametric study of these data conducted at Langley with a large computer program are presented. These categories for sharp cones have 568, 67, and 77 data points, respectively. This study is essentially a refinement and extension of the corresponding work presented at the 1967 San Bernardino meeting (ref. 4). The general objective of this study is to minimize the sigma deviation from least-square curve fits of the data in each of the three categories of tests. Four transition Reynolds number parameters of the following form have been used:

$$\left. \begin{array}{l} \mathrm{I} = \log_{10}\left(\dfrac{R_{x,t}}{R^n}\right) \\[2em] \mathrm{II} = \log_{10}\left(\dfrac{R_{x,t}}{R_D{}^n}\right) \\[2em] \mathrm{III} = \log_{10}\left(\dfrac{R_{\delta^*,t}}{R^n}\right) \\[2em] \mathrm{IV} = \log_{10}\left(\dfrac{R_{\delta^*,t}}{R_D{}^n}\right) \end{array} \right\} \tag{4}$$

where δ^* is computed by the local-similarity formula given in reference 4. Hence, these values of δ^* cannot be regarded as true physical values of displacement thickness but rather as values computed from this specified function (ref. 4) of local Reynolds number, Mach number, and h_w/h_e.

Each of these transition Reynolds number parameters has been plotted against the local flow parameters

$$\left. \begin{array}{l} M_e \\[1em] F_1 = M_e\left(\dfrac{h_w}{h_e}\right)^{0.7\exp\left(-0.05M_e{}^2\right)} \\[2em] F_2 = \displaystyle\sum_{i=0}^{m}\left[\left(\sum_{j=0}^{k} a_{ij}M_e{}^j\right)\left(\dfrac{h_w}{h_e}\right)^i\right] \end{array} \right\} \tag{5}$$

The principal results of the study are given in table II with typical plots shown in figure 17. (Only 60 of the 77 data points used to obtain the flight data correlations are shown in the figure.) Linear and quadratic curve fits of the transition parameters (eqs. (4)) as functions of M_e and F_1 have been obtained. The polynomial coefficients for these curve fits and the values of n in equations (4) that resulted in the three smallest values of σ_x are given in table II(a) for each of the categories of tests (wind tunnel, ballistic range, free flight, and all data). For the I and II parameters of equa-

18

tions (4), the values of σ_x shown in table II and figure 17 are the deviations in terms of the fraction of a log cycle. However, for the III and IV parameters, σ_x is twice the standard deviation (used again as the fraction of a log cycle) to account for the fact that x_t is proportional to $\left(\delta_t^*\right)^2$ and thereby to allow direct comparison of all σ_x values.

Given in table II(b) are the a_{ij} matrix coefficients for F_2 and the coefficients for linear fits of the transition parameters with F_2. These relations may be written in the general functional form

$$\log_{10}\left(\frac{R_{L_1}}{R_{L_2}^n}\right) = A + BF_2 \tag{6}$$

where L_1 is either x_t or δ_t^* and L_2 is either 1 foot or the base diameter of the cones. The a_{ij} coefficients were obtained by first plotting the transition parameters (eqs. (4)) against h_w/h_e for selected narrow ranges in local Mach number M_e. Then, quadratic curve fits of the form

$$\log_{10}\left(\frac{R_{L_1}}{R_{L_2}^n}\right) = \sum_{i=0}^{2} b_i \left(\frac{h_w}{h_e}\right)^i \tag{7}$$

were obtained for each narrow range in M_e with constant values of b_i determined by the method of least squares. Auxiliary plots of b_i against M_e then established the values of the a_{ij} coefficients where

$$b_i = \sum_{j=0}^{k} a_{ij} M_e^{\,j} \tag{8}$$

In general, the values of σ_x are reduced successively by the use of M_e, F_1, and F_2 in that order. (See table II and fig. 17.) In particular, the F_2 parameter appears to result in significantly smaller values of σ_x for the wind-tunnel data (where the minimum value of σ_x was 0.140). This result presumably reflects the greater flexibility of the F_2 parameter in accounting for the dependence of wind-tunnel transition data on M_e and h_w/h_e. The use of the F_2 parameter also gave the minimum σ_x values of 0.141 and 0.160 for the free-flight and all-data categories, respectively. The minimum value of σ_x for the ballistic-range data was 0.100 obtained with the F_1 and III parameters.

It is also worth noting that the use of a base-diameter Reynolds number (expressions II and IV in eqs. (4)) generally gives small deviations for the wind-tunnel, free-flight, and all-data categories. This result may indicate the influence of some scale parameter that is roughly related to the size of the test model. In wind-tunnel tests, the size of the test model is often determined by the tunnel size, which, in turn, may be related back to sound disturbance levels. (See fig. 3.)

It is of interest to determine the values of x_t computed from these correlation equations for a given set of data. For this purpose, several transition data points from the Reentry F flight are compared with typical correlations in figure 18. (The original set of data used to obtain the correlations consisted of 77 data points, including eight points from the Reentry F flight; 60 of these original data points are shown in the figure.) It is seen that the Reentry F data generally fall within the $\pm\sigma_x$ band and that the F_1 correlation for flight data (fig. 18(a)) would give the best prediction for the Reentry F conditions on the basis of σ_x. (For comparison, these Reentry F data points are also identified in fig. 17 on the F_1 plot for flight data where $\sigma_x = 0.144$.) The maximum deviation of the data from the curve fit in the range of $6 < F_1 < 14$ is -0.154 of a log cycle. For the Reentry F flight, this correlation equation would have predicted x_t with an error of 1.2 meters (4 ft) too far aft for typical conditions. On the other hand, the correlation of figure 18(b) with a deviation of 0.2 of a log cycle would have predicted transition too far forward by about 1 meter (3.3 ft) at the same typical condition. These sample calculations indicate that a correlation with a minimum σ_x deviation may not give the most reliable x_t predictions for a given set of data. In this particular situation, the larger value of σ_x represents an x_t prediction that would be forward of the actual x_t data, thereby a smaller absolute error results because

$$\frac{(x_t)_{\text{data}}}{(x_t)_{\text{predicted}}} = 10^{\sigma_x}$$

Another application of the sharp-cone correlations to flight conditions is illustrated in figure 19. Shown are predictions for length of laminar run on a cone at zero angle of attack from the flight data correlations indicated in table II(a). For reference purposes, surface conditions on the cone are considered to be the same as those for a flat plate in flight at the angles of attack, free-stream Mach numbers, and free-stream dynamic pressures shown. Transition location predictions differ by factors of 3 or 4 at the lower dynamic pressures, depending on the parameters used. However, flight data, upon which the correlations are based, do not exist below a dynamic pressure of roughly 48 000 N/m^2 (1000 lb/ft^2). The reliability of the correlations in flow regions beyond the original data is therefore questionable.

20

For illustrative purposes, the σ_x deviation bands for $M_\infty = 6$ are also shown in figure 19. At the larger dynamic pressures where the correlations are more reliable, the deviation bands from correlations I and III overlap. However, at the lower dynamic pressures, the maximum predictions for x_t from correlation I are less than the minimum x_t values from correlation III. Note also that standard-deviation errors in predictions for x_t increase as x_t increases, because of the definition of σ_x in terms of logarithmic parameters. The standard-deviation errors are constant but unequal in magnitude for positive and negative deviations about the mean fitted curve. This result is apparent from the relation for the standard deviation Δx_t written as

$$\pm \frac{\left(x_t\right)_{\text{deviation}}}{\left(x_t\right)_{\text{mean}}} = 10^{\pm \sigma_x} - 1$$

This relation is derived from the general definition of σ_x applied to a sharp cone where flow properties are constant along the cone.

Correlations for Blunt Cones at $\alpha \approx 0^0$

The blunt-cone data are identified by + symbols in figure 17. The blunt-cone criterion is identical with that used in reference 4. In most cases, these blunt-cone data are best correlated by the transition parameters III and IV against the local flow parameters M_e and F_1.

Correlations for Various Shapes at Large α

The blunt-cone correlations for $\alpha \approx 0^0$ considered in the previous section of this report have been utilized by Johnson (ref. 26) as correlations for transition on the windward symmetry line of cones, delta wings, and space shuttle configurations at large angle of attack. Recent data compiled by E. Leon Morrisette of Langley from wind-tunnel tests on three shuttle configurations are shown in figure 20, which utilizes the same parameters of reference 26 and includes data from Langley Mach 8 tests and from a cone flight test at large angle of attack (ref. 27). The solid line represents the best linear fit to 78 flight data points for sharp cones at $\alpha = 0^0$ and was established independently of any other data presented in figure 20 by methods of the previous section. (See table II(a).) In general, the cone angle-of-attack flight data scatter around the linear fit to the 78 flight data points from $M_e = 5$ to 12. Below a local Mach number of 5, the data drop sharply from the $\alpha = 0^0$ linear fit. The edge conditions are calculated by using oblique-shock entropy. The method of determining $R_{\delta^*,t}$ is presented in reference 4.

For $M_e < 5$, the data in this correlation scatter over 0.4 of a log cycle in the $R_{\delta^*,t}$ parameter. In terms of x_t this scatter results in a maximum uncertainty band of

approximately 0.8 of a log cycle or a factor of 6.3 in $R_{x,t}$. Clearly, these data are not satisfactorily correlated by these parameters, and the results should only be used to establish a lower limit, or a sort of minimum transition distance. This minimum transition distance would then correspond to the most forward position of transition observed for the configurations and test conditions of figure 20. Since the unit Reynolds number is an important parameter in this correlation, extrapolation to conditions for outside the range of data conditions must be done with caution, as illustrated by the results of figure 19.

Some of the same data of figure 20 and some additional data are shown in figure 21, adapted by E. Leon Morrisette from a compilation by Jerry N. Hefner as given in slide 2 of reference 28. Hefner used the concept of a local angle of attack α_w, and all data were reduced with normal-shock entropy. The criteria for data reduction used herein are based on oblique-shock entropy. The roughly 45° slope of $R_{x,t}$ with R (fig. 21(a)) for many of the test results indicates that transition sometimes sticks at a fixed location as R is increased.

Hefner's lower bound for transition is shown in figure 21(b) where oblique-shock entropy has been used. For applications of these various correlations to typical space shuttle trajectories, see reference 26.

EFFECTS OF SMALL ANGLE OF ATTACK

Transition Detection Techniques on Cones at Small α

Reference 4 showed transition results on a cone at incidence which seemed to be at odds with previously accepted transition behavior (e.g., ref. 29). These results also appeared later in the literature. (See ref. 30.) This conflicting behavior was attributed to the large local Mach number changes caused by angle of attack and the subsequent effect of this local Mach number change on transition. These results have been reexamined by Fischer and Rudy (ref. 31), who tested a cone of identical geometry in the same facility. As shown in figure 22(a), their results do not agree with those previously obtained by Maddalon and Henderson (ref. 30), with a major disagreement involving the trend of transition on the leeward side of the cone. In reference 30 detection of transition involved the use of a surface pitot probe at a fixed location, and that of reference 31 used thermocouples which covered the length of the cone. Tunnel supply pressure was varied in order to establish the Reynolds number at which the fixed surface pitot probe indicated transition in the investigation of reference 30; thus, both the acoustic radiated pressure intensity and model boundary-layer thickness were different where transition occurred at different supply pressures. Besides this factor, other effects are probably major contributors to the disagreement.

The significant forward movement on the windward ray reported by Maddalon and Henderson is now believed to be erroneous and due to a combination of a relatively thin boundary layer and a large pitot-probe diameter. For example, at an angle of attack of 2° the ratio of probe diameter to local boundary-layer thickness was about 0.3. This ratio suggests a too large surface pitot probe which (1) sensed an increase in pitot pressure due to averaging over too large a volume or (2) produced local separation of the boundary layer rather than detecting the onset of transition. Another possibility associated with finite surface pitot-probe size is that the probe sensed transition effects in the boundary layer away from the wall which, as yet, had no effect on the wall heating. Another section of this paper considers the effects of this "precursor" transition phenomenon on boundary-layer characteristics.

On the leeward side, recent oil-flow studies by Fischer show incipient separation at 2° angle of attack at the location of the surface pitot probe which could explain Maddalon and Henderson's erroneous reading there. These conflicting results illustrate the care which must be exercised in the use of instrumentation and the interpretation of transition results.

Another effect of the technique used to locate transition was discovered by careful examination of the Reentry F flight data. The usual procedure for identifying transition from flight data is to locate the time on the temperature-time plots where the temperature starts to increase rather abruptly. In figure 22(b) (from ref. 24) the results from this usual procedure are compared with alternate approaches based on the heating-rate distribution with x and the heating-rate history. The latter two methods give transition locations up to 1 meter (3 ft) farther forward than the former and more common technique. Smaller values of $R_{\delta^*,t}$ are then obtained with the latter methods which were used for the Reentry F data in figures 17 and 18. These data should then be lower than most other flight data, as confirmed by figures 17 and 18(a), where F_1 is the local flow parameter. (A detailed analysis of the Reentry F transition and heat-transfer data is given in ref. 32.)

Effect of Small Angle of Attack on Transition

The thermocouple data of figure 22(a) are replotted in figure 22(c), which includes unpublished thermocouple data obtained by Stainback on the prime meridian of a 5° half-angle cone in the Langley Mach 8 variable-density hypersonic tunnel. Values of $\dfrac{x_t}{x_{t,\alpha=0°}}$ on the windward side generally decrease with increasing nose-radius Reynolds number $R_{\infty,r}$ except for the data from reference 31 (helium flow at a much larger Mach number). On the leeward side, there appears to be a peak in the variation of $\dfrac{x_t}{x_{t,\alpha=0°}}$ with $R_{\infty,r}$ at $R_{\infty,r} = 16.6 \times 10^3$, again with the exception of the data from reference 31. For these

wind-tunnel data, it can be tentatively concluded that $R_{\infty,r}$ is a major parameter affecting transition for $\left|\dfrac{\alpha}{\theta_c}\right| \leqq 0.35$.

HYPERSONIC "PRECURSOR" TRANSITION

Results from hot-wire and hot-film studies indicate that significant oscillations occur in the boundary layer away from the wall far upstream of the transition location given by wall instrumentation. Such behavior is evident in the turbulence profiles with fixed unit Reynolds number presented in reference 4 based on the data of references 33 and 34. Fischer and Weinstein have recently examined this problem at a local Mach number of 14 on the 2.87° cone in the Langley Mach 20 high Reynolds number helium tunnel utilizing visual evidence, pitot-pressure surveys, and wall thermocouple instrumentation (ref. 35). They found that appreciable waviness at the boundary-layer edge, indicative of large oscillations, appeared upstream at a distance from the tip as little as about 40 percent of the distance to transition given by the wall instrumentation. A total spreading angle for the mean disturbances can be crudely determined as 0.85°, or relative to the wall 0.6°, assuming that the disturbances initiate at the critical layer (ref. 36), or 95 percent of the boundary-layer height, as shown in figure 23. An examination of the available data for Mach numbers from 2.5 to 14 indicates the spreading angle relative to the wall is approximately 0.5° to 1°. Since both the critical layer moves outward in the boundary layer and the boundary-layer thickness increases with increasing Mach number, the relatively constant spreading angle implies a greater "upstream influence" of boundary-layer transition as Mach number increases.

The initial turbulence location is believed to be important since the mean properties of the boundary layer can be affected from this point downstream. Additionally, the eddy viscosity, intermittency, and so forth, which govern the disturbance growth from the outer transition location down to the wall must be properly modeled in order to compute the mean properties of transitional-turbulent boundary-layer development (for instance, by the method of ref. 22). At low speeds, the large upstream oscillations in the boundary layer apparently do not influence the mean laminar velocity profiles or the thickness parameters δ, δ^*, and θ, since good agreement with the laminar Blasius solution has been obtained (refs. 18 and 37). However, at high speeds larger oscillations occur ahead of the transition location. Indeed, Fischer and Weinstein found a large influence on the mean boundary-layer profiles in this investigation. One survey obtained at 80 percent of the streamwise distance to the wall transition location indicated that the outer part of the boundary layer was transitional as expected from the visual evidence (spark schlieren) and the boundary-layer thickness was about 15 percent greater than the prediction from a

laminar similar solution. A profile taken a short distance downstream of the indicated wall transition location $\left(x_{survey} = 1.13x_{transition}\right)$ showed a well-developed transitional profile. An examination of boundary-layer mean profiles labeled laminar by previous investigators (refs. 38 to 40) at hypersonic Mach numbers suggests a transitional outer profile as in this latest investigation. The numerical methods which compute the development of boundary-layer profiles and thickness parameters given some upstream initial conditions may not provide good profile or thickness predictions for hypersonic flows of this type. Because the transition process initiates in the outer part of the boundary layer, a means of specifying this initial location and downstream development of mean turbulence in the computation methods must be devised.

TRANSITION IN FREE SHEAR LAYERS

A recent investigation of transition and heat transfer in free shear layers within a hypersonic flow field was conducted by Stanley F. Birch at Langley. The free shear layer was generated by impingement of a two-dimensional wedge shock upon the bow shock of a blunt two-dimensional body. A schlieren photograph of the resulting flow field is given in figure 24. The flow conditions of the experiment are given in the figure.

The Reynolds numbers for transition based on the length from the origin of the shear layer and the flow conditions on the high-velocity side of the layer, as illustrated in the photograph in figure 24, are plotted against M_2 in the lower part of figure 24. Shown for comparison are transition Reynolds numbers for separated boundary layers from reference 41. The present data show transition at a lower Reynolds number, by about a factor of 2, than the data of reference 41. The reason for this difference can probably be attributed to the small initial thickness of the shear layer.

CONCLUDING REMARKS

Measurements in different air wind tunnels of transition locations on sharp cones and of the corresponding surface pressure fluctuations upstream of transition have established that transition depends inversely on the root-mean-square noise disturbances provided that all other test conditions are nearly the same. Hot-wire and transition measurements in the 150-cm (60-in.) leg (Mach 18) of the Langley Mach 20 high Reynolds number helium tunnel in the free stream and shock layer of a 2.87° cone have shown: (1) The disturbances are predominantly sound radiated from the tunnel-wall turbulent boundary layers — with the same inverse effect on transition as in air, and (2) the normalized disturbance levels remain approximately constant across this weak shock. Hot-wire measurements obtained in the Langley 22-inch helium tunnel in the free stream and shock layer of a 16° cone give the same results as item (1) in the 150-cm (60-in.) facility.

Also, the root-mean-square sound levels from surface pressure transducers are approximately equal to those from hot wires in the shock layers. However, the stronger shock of the 16° cone caused a 25-percent reduction in the normalized disturbance levels behind the shock. Comparison of previous transition and sound results with the present results obtained from surface pressure transducers and from hot-wire data suggests that transition Reynolds numbers in wind tunnels are also dependent on parameters governing the characteristics of the laminar profile, such as local Mach number, wall-to-total temperature ratio, and test gas.

The variation of transition Reynolds number with unit Reynolds number has been reasonably well predicted by a finite-difference procedure which utilized a relation between acoustic pressure and velocity disturbances that included one arbitrary constant.

A concept for a laminar flow suction shield with longitudinal slots has been tested in the Langley Mach 8 variable-density hypersonic wind tunnel. The results show that suction moves transition aft by a factor of at least 4 and reduces radiated noise by 20 to 30 percent.

Correlations of transition data on cones at zero angle of attack have been optimized for minimum sigma deviation from least-square curve fits of data from the three categories of tests: wind tunnel, ballistic range, and free flight. The minimum sigma deviations in terms of the fraction of a log cycle for the actual longitudinal locations of transition were 0.140, 0.100, and 0.141, respectively. The minimum deviation for correlations of all data was 0.160.

Wind-tunnel transition data for slightly blunted cones at small angle of attack indicate that transition on the windward side moves forward with increasing Reynolds number based on nose-tip radius. On the leeward side, transition first moves to the rear as this Reynolds number is increased up to about 1.7×10^4, then transition moves forward with further increases in the Reynolds number.

Studies of transition data on cones, delta wings, and space shuttle configurations at large angle of attack indicate that, in many cases, transition tends to stick at a fixed station on the windward symmetry line as the unit Reynolds number is increased. Also, the large spread in the data in spite of correlation attempts indicates that only a minimum transition Reynolds number can be used with confidence for these types of configurations.

Transition appears in the outer part of hypersonic boundary layers far upstream of the first indication at the wall. This "precursor" transition must be incorporated into boundary calculation procedures and must be taken into account in interpreting transition results.

Langley Research Center,
National Aeronautics and Space Administration,
Hampton, Va., May 26, 1972.

REFERENCES

1. Hamilton, H. Harris: Turbulent Heating on Space Shuttle Orbiters During Reentry. Space Transportation System Technology Symposium, NASA TM X-52876, Vol. I, 1970, pp. 463-483.

2. Martellucci, A.: Asymmetric Transition Effects on the Static Stability and Motion History of a Slender Vehicle. SAMSO TR-70-141, U.S. Air Force, Jan. 1970. (Available from DDC as AD 872 219L.)

3. Pate, S. R.; and Schueler, C. J.: The Influence of Radiated Aerodynamic Noise on Model Boundary-Layer Transition in Supersonic and Hypersonic Wind Tunnels. Boundary Layer Transition Study Group Meeting, William D. McCauley, ed., BSD-TR-67-213, Vol III, U.S. Air Force, Aug. 1967, pp. 21-i − 21-40. (Available from DDC as AD 384 006.)

4. Bertram, Mitchel H.; and Beckwith, Ivan E.: NASA-Langley Boundary Layer Transition Investigations. Boundary Layer Transition Study Group Meeting, William D. McCauley, ed., BSD-TR-67-213, Vol III, U.S. Air Force, Aug. 1967, pp. 18-i − 18-74. (Available from DDC as AD 384 006.)

5. Stainback, P. C.; Fischer, M. C.; and Wagner, R. D.: Effects of Wind-Tunnel Disturbances on Hypersonic Boundary-Layer Transition. Pts. I and II. AIAA Paper No. 72-181, Jan. 1972.

6. Stainback, P. C.: Hypersonic Boundary-Layer Transition in the Presence of Wind-Tunnel Noise. AIAA J., vol. 9, no. 12, Dec. 1971, pp. 2475-2476.

7. Pate, S. R.; and Schueler, C. J.: Radiated Aerodynamic Noise Effects on Boundary-Layer Transition in Supersonic and Hypersonic Wind Tunnels. AIAA J. vol. 7, no. 3, Mar. 1969, pp. 450-457.

8. Wagner, R. D., Jr.; Maddalon, D. V.; and Weinstein, L. M.: Influence of Measured Freestream Disturbances on Hypersonic Boundary-Layer Transition. AIAA J., vol. 8, no. 9, Sept. 1970, pp. 1664-1670.

9. Laufer, John: Factors Affecting Transition Reynolds Numbers on Models in Supersonic Wind Tunnels. J. Aeronaut. Sci., vol. 21, no. 7, July 1954, pp. 497-498.

10. Laufer, John: Aerodynamic Noise in Supersonic Wind Tunnels. J. Aerosp. Sci., vol. 28, no. 9, Sept. 1961, pp. 685-692.

11. Kendall, J. M., Jr.: Supersonic Boundary Layer Transition Studies. Supporting Research and Advanced Development, Space Programs Summary 37-62, Vol. III, Jet Propulsion Lab., California Inst. Technol., Apr. 30, 1970, pp. 43-47.

12. Pate, S. R.: Measurements and Correlations of Transition Reynolds Numbers on Sharp Slender Cones at High Speeds. AIAA J., vol. 9, no. 6, June 1971, pp. 1082-1090.

13. Morkovin, Mark V.: Critical Evaluation of Transition From Laminar to Turbulent Shear Layers With Emphasis on Hypersonically Traveling Bodies. AFFDL-TR-68-149, U.S. Air Force, Mar. 1969. (Available from DDC as AD 686 178.)

14. Wagner, R. D.: Hot Wire Measurements of Freestream and Shock Layer Disturbances. AIAA J., vol. 9, no. 12, Dec. 1971, pp. 2468-2470.

15. Morkovin, Mark V.: Fluctuations and Hot Wire Anemometry in Compressible Flows. AGARDograph 24, Nov. 1956.

16. Dryden, Hugh L.: Air Flow in the Boundary Layer Near a Plate. NACA Rep. 562, 1936.

17. Hall, A. A.; and Hislop, G. S.: Experiments on the Transition of the Laminar Boundary Layer on a Flat Plate. R. & M. No. 1843, British A.R.C., 1938.

18. Schubauer, G. B.; and Skramstad, H. K.: Laminar-Boundary-Layer Oscillations and Transition on a Flat Plate. NACA Rep. 909, 1948.

19. McDonald, H.; and Fish, R. W.: Practical Calculations of Transitional Boundary Layers. Rep. L110887-1, Res. Lab., United Aircraft Corp., Mar. 1972.

20. Groth, E. E.: Boundary Layer Suction Experiments at Supersonic Speeds. Boundary Layer and Flow Control. Vol. 2, G. V. Lachmann, ed., Pergamon Press, Inc., 1961, pp. 1049-1076.

21. Jones, Robert A.; and Hunt, James L.: Use of Fusible Temperature Indicators for Obtaining Quantitative Aerodynamic Heat-Transfer Data. NASA TR R-230, 1966.

22. Harris, Julius E.: Numerical Solution of the Equations for Compressible Laminar, Transitional, and Turbulent Boundary Layers and Comparisons With Experimental Data. NASA TR R-368, 1971.

23. Mack, Leslie M.: Computation of the Stability of the Laminar Compressible Boundary Layer. Vol. 4 of Methods in Computational Physics, Berni Alder, Sidney Fernbach, and Manuel Rotenberg, eds., Academic Press, Inc., 1965, pp. 247-299.

24. Wright, Robert L.; and Zoby, Ernest V.: Flight Measurements of Boundary-Layer Transition on a 5° Half-Angle Cone at a Free-Stream Mach Number of 20 (Reentry F). NASA TM X-2253, 1971.

25. Johnson, Charles B.; Stainback, P. Calvin; Wicker, Kathleen C.; and Boney, Lillian R.: Boundary-Layer Edge Conditions and Transition Reynolds Number Data for a Flight Test at Mach 20 (Reentry F). NASA TM X-2584, 1972.

26. Johnson, Charles B. (With appendix B by George C. Ashby, Jr.): Boundary-Layer Transition and Heating Criteria Applicable to Space Shuttle Configurations From Flight and Ground Tests. Vol. I of NASA Space Shuttle Technology Conference, NASA TM X-2272, 1971, pp. 97-156.

27. Haigh, Wayne W.; Lake, Bruce M.; and Ko, Denny R. S.: Analysis of Flight Data on Boundary Layer Transition at High Angles-of-Attack. NASA CR-1913, 1972.

28. Masek, R. V.; and Forney, J. Alan: An Analysis of Predicted Space Shuttle Temperatures and Their Impact on Thermal Protection Systems. Vol. I of NASA Space Shuttle Technology Conference, NASA TM X-2272, 1971, pp. 75-96.

29. Bertram, Mitchel H.; and Henderson, Arthur, Jr.: Effects of Boundary-Layer Displacement and Leading-Edge Bluntness on Pressure Distribution, Skin Friction, and Heat Transfer of Bodies at Hypersonic Speeds. NACA TN 4301, 1958.

30. Maddalon, Dal V.; and Henderson, Arthur, Jr.: Hypersonic Transition Studies on a Slender Cone at Small Angles of Attack. AIAA J., vol. 6, no. 1, Jan. 1968, pp. 176-177.

31. Fischer, M. C.; and Rudy, D. H.: Effect of Angle of Attack on Boundary-Layer Transition at Mach 21. AIAA J., vol. 9, no. 6, June 1971, pp. 1203-1205.

32. Stainback, P. Calvin; Johnson, Charles B.; Boney, Lillian R.; and Wicker, Kathleen C.: Theoretical Prediction of Heat-Transfer Measurements of a Flight Experiment at Mach 20 (Reentry F). NASA TM X-2560, 1972.

33. Potter, J. Leith; and Whitfield, Jack D.: Effects of Unit Reynolds Number, Nose Bluntness, and Roughness on Boundary Layer Transition. AEDC-TR-60-5, U.S. Air Force, Mar. 1960.

34. Staylor, W. F.; and Morrisette, E. L.: Use of Moderate-Length Hot Wires To Survey a Hypersonic Boundary Layer. AIAA J., vol. 5, no. 9, Sept. 1967, pp. 1698-1700.

35. Fischer, M. C.; and Weinstein, L. M.: Cone Transitional Boundary-Layer Structure at $M_e = 14$. AIAA J., vol. 10, no. 5, May 1972, pp. 699-701.

36. Stainback, P. Calvin: Use of Rouse's Stability Parameter in Determining the Critical Layer Height of a Laminar Boundary Layer. AIAA J., vol. 8, no. 1, Jan. 1970, pp. 173-175.

37. Schubauer, G. B.; and Klebanoff, P. S.: Contributions on the Mechanics of Boundary-Layer Transition. NACA Rep. 1289, 1956. (Supersedes NACA TN 3489.)

38. Bertram, Mitchel H.:   Exploratory Investigation of Boundary-Layer Transition on a Hollow Cylinder at a Mach Number of 6.9.   NACA Rep. 1313, 1957.   (Supersedes NACA TN 3546.)

39. Maddalon, Dal V.; and Henderson, Arthur, Jr.:   Boundary-Layer Transition on Sharp Cones at Hypersonic Mach Numbers.   AIAA J., vol. 6, no. 3, Mar. 1968, pp. 424-431.

40. Softley, E. J.; Graber, B. C.; and Zempel, R. E.:   Experimental Observation of Transition of the Hypersonic Boundary Layer.   AIAA J., vol. 7, no. 2, Feb. 1969, pp. 257-263.

41. Chapman, Dean R.; Kuehn, Donald M.; and Larson, Howard K.:   Investigation of Separated Flows in Supersonic and Subsonic Streams With Emphasis on the Effect of Transition.   NACA Rep. 1356, 1958.   (Supersedes NACA TN 3869.)

TABLE I.- CONE TRANSITION EXPERIMENT[a]

$[M_e = 5]$

Name of facility	Symbol[b]	Tunnel size	M_∞	T_o K	T_o °R	θ_c, deg	T_w/T_o	Test gas
Langley 20-inch Mach 6 tunnel	○	50-cm (20-in.) square	6	500	900	10	0.6	Air
Mach 6 high Reynolds number tunnel	◇	30-cm (12-in.) diameter	6	500	900	10	0.6	Air
Mach 8 variable-density hypersonic tunnel	□	46-cm (18-in.) diameter	8	830	1500	16	0.4	Air
Langley 22-inch helium tunnel	△	56-cm (22-in.) diameter	20	300 to 500	550 to 900	16	1.0, 0.6	Helium

aFrom reference 5.
bUsed in figures 3, 4, and 5.

31

TABLE II.- CORRELATION PARAMETERS AND CURVE-FIT COEFFICIENTS FOR MINIMUM σ_x RESULTS

(a) Transition parameters as functions of M_e and F_1

| Test category	Data points	Transition parameter	Local flow parameter	σ_x	n (eqs. (4))	Polynomial coefficients in ascending order		
						0	1	2
Wind tunnel	568	III	[a]M_e	0.160	0.175	2.1996E+00	7.9555E-02	3.7262E-03
		III	M_e	.165	.150	2.2634E+00	1.2335E-01	0
		IV	[a]M_e	.166	.175	2.3058E+00	8.5177E-02	1.7664E-03
		IV	F_1	.161	.225	2.0238E+00	2.9862E-02	6.7987E-03
		II	F_1	.164	.500	4.0387E+00	-2.4037E-01	1.9218E-02
		III	F_1	.166	.225	1.9378E+00	2.7706E-04	1.0978E-02
Ballistic range	67	I	M_e	0.123	0.700	2.1441E+00	-2.1870E-01	1.9522E-02
		III	[a]M_e	.126	.325	8.4763E-01	9.5650E-02	2.7718E-03
		III	M_e	.127	.325	7.6631E-01	1.2696E-01	0
		III	F_1	.100	.250	1.3618E+00	1.3126E-01	-4.3203E-04
		III	[a]F_1	.100	.250	1.3728E+00	1.2664E-01	0
		IV	F_1	.119	.150	2.2518E+00	1.2222E-01	1.7089E-03
Free flight	77	I	[a]M_e	0.151	0.650	2.5625E+00	-6.4743E-03	4.2861E-03
		III	[a]M_e	.156	.350	1.0191E+00	1.4018E-01	-1.4686E-03
		I	M_e	.157	.700	2.0294E+00	6.2987E-02	0
		IV	[a]F_1	.144	.325	1.2496E+00	1.1096E-01	-4.0979E-04
		IV	F_1	.145	.325	1.2683E+00	1.0441E-01	0
		I	F_1	.152	.600	2.9444E+00	-2.0261E-02	5.0315E-03
		III	[b]F_1	.154	.225	1.9042E+00	1.1667E-01	0
		I	[c]F_1	.154	.700	2.22443E+00	-1.68565E-02	5.22154E-03
		III	[c]F_1	.152	.250	1.67638E+00	1.34369E-01	-9.85912E-04
	78	III	[d]M_e	.172	.250	1.79411E+00	1.12288E-01	0
All data	712	IV	M_e	0.184	0.225	1.9955E+00	8.6549E-02	1.3681E-03
		IV	M_e	.186	.225	1.9487E+00	1.0467E-01	0
		II	M_e	.198	.650	2.6729E+00	-9.1632E-02	8.7703E-03
		IV	F_1	.179	.275	1.6127E+00	7.5949E-02	2.6979E-03
		IV	F_1	.184	.300	1.3488E+00	1.1262E-01	0
		II	F_1	.189	.650	2.9900E+00	-1.7941E-01	1.3825E-02

[a]Plotted in figure 17.
[b]Used for figure 18(a).
[c]Used for figure 19.
[d]Figure 20.

TABLE II.- CORRELATION PARAMETERS AND CURVE-FIT COEFFICIENTS FOR MINIMUM σ_x RESULTS – Concluded

(b) Transition parameters as functions of F_2

Test category	Data points	Transition parameter	σ_x	n (eqs. (4))	Coefficients of linear curve fit		a_{ij} matrix coefficients			
					A	B	j = 0	j = 1	j = 2	i
Wind tunnel	568	a_I	0.140	0.300	0.72861	0.83615	5.6277E+00 -3.4897E-01 -7.6639E-02	-3.8293E-01 1.4557E-01 5.9694E-03	3.2814E-02 -1.1790E-02 2.6947E-04	0 1 2
		II	0.143	0.400	1.02110	0.74013	4.2658E+00 -8.7410E-02 -3.9560E-02	1.6061E-02 1.5942E-03 4.8735E-03	0 0 0	0 1 2
		a_{IV}	0.150	0.225	0.11168	0.94935	1.6002E+00 2.7641E-01 -4.2888E-02	1.4207E-01 -3.2828E-02 5.4027E-03	0 0 0	0 1 2
Ballistic range	67	a_{III}	0.104	0.3	-0.0409	0.94799	7.8443E-01 4.0007E-01 -7.2634E-02	1.6544E-01 -4.4229E-02 8.9108E-03	0 0 0	0 1 2
		I	0.119	0.7	0.40118	0.66353	2.7652E+00 4.7868E-02 -1.2184E-01	-4.0386E-01 3.2978E-02 1.9038E-02	3.6374E-02 -4.1439E-03 -5.8255E-04	0 1 2
Free flight	77	a_{III}	0.141	0.275	0.75352	0.74794	7.3825E-01 4.1157E-01 -7.2747E-02	1.9448E-01 -4.6494E-02 8.7124E-03	0 0 0	0 1 2
		IV	0.154	0.325	0.16352	0.92425	1.0247E+00 2.1626E-01 -2.6918E-02	1.3254E-01 -2.6167E-02 3.7966E-03	0 0 0	0 1 2
All data	712	IV	0.160	0.250	0.11807	0.94817	1.4563E+00 2.6137E-01 -3.8896E-02	1.3968E-01 -3.1163E-02 5.0011E-03	0 0 0	0 1 2
		II	0.169	0.550	0.45694	0.85313	3.3851E+00 -1.6081E-01 -1.7765E-02	3.8676E-03 9.8216E-03 2.6527E-03	0 0 0	0 1 2
		b_{III}	0.208	0.175	0.42352	0.86087	1.5014E+00 3.9604E-01 -6.6445E-02	1.8584E-01 -4.5943E-02 8.0509E-03	0 0 0	0 1 2

[a]Plotted in figure 17.
[b]Used for figure 18(b).

33

θ_c, deg	s in.	cm
10	4	10.16
16-18.35	3	7.62

TURBULENT BOUNDARY LAYER

CONE BOUNDARY LAYER

TURBULENT

LAMINAR

PRESSURE TRANSDUCERS

θ_c

s

HOT-WIRE PROBES

M_e

M_∞

ACCELEROMETER

MACH LINE FROM FIXED DISTURBANCE

ENVELOPE OF SOUND WAVES FROM MOVING SOURCES IN TUNNEL-WALL BOUNDARY LAYER
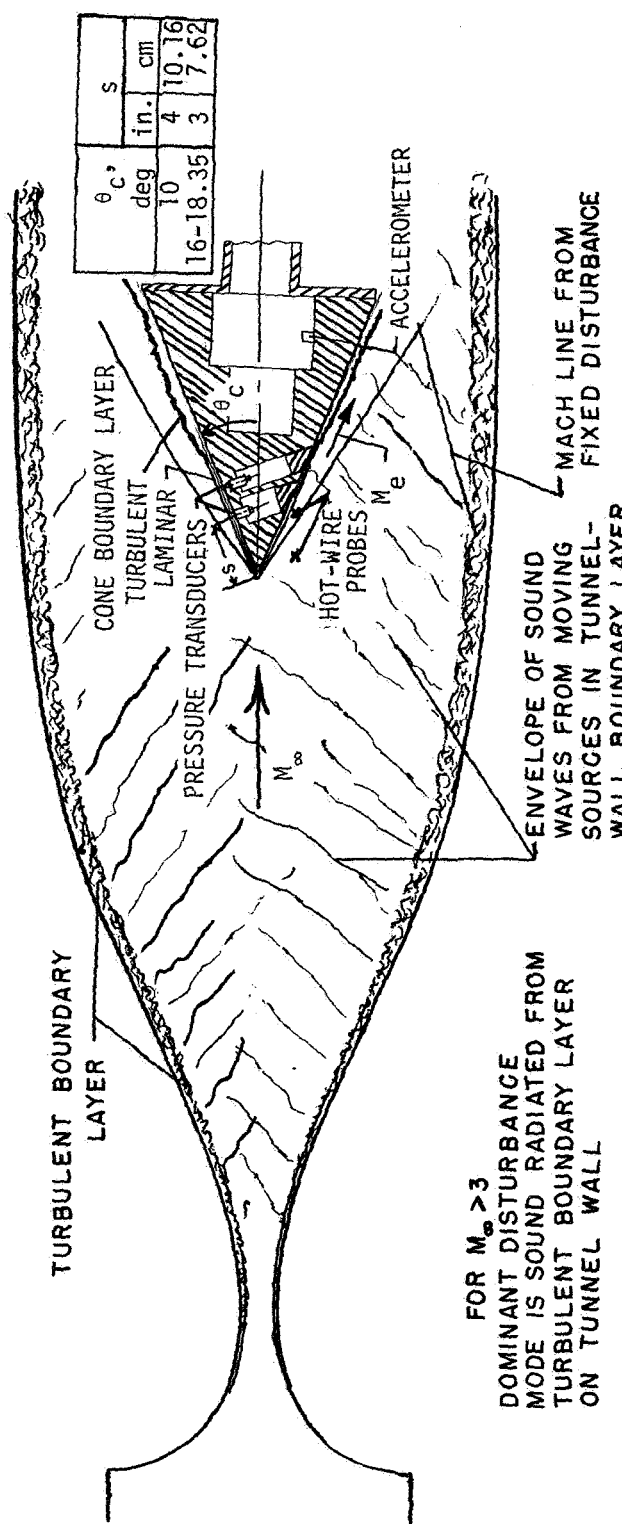
FOR $M_\infty > 3$

DOMINANT DISTURBANCE MODE IS SOUND RADIATED FROM TURBULENT BOUNDARY LAYER ON TUNNEL WALL

Figure 1.- Measurements of transition location, surface sound pressures, and hot-wire fluctuations in shock layer and free stream.

34

Free stream, M_∞ = 17.1 to 17.7
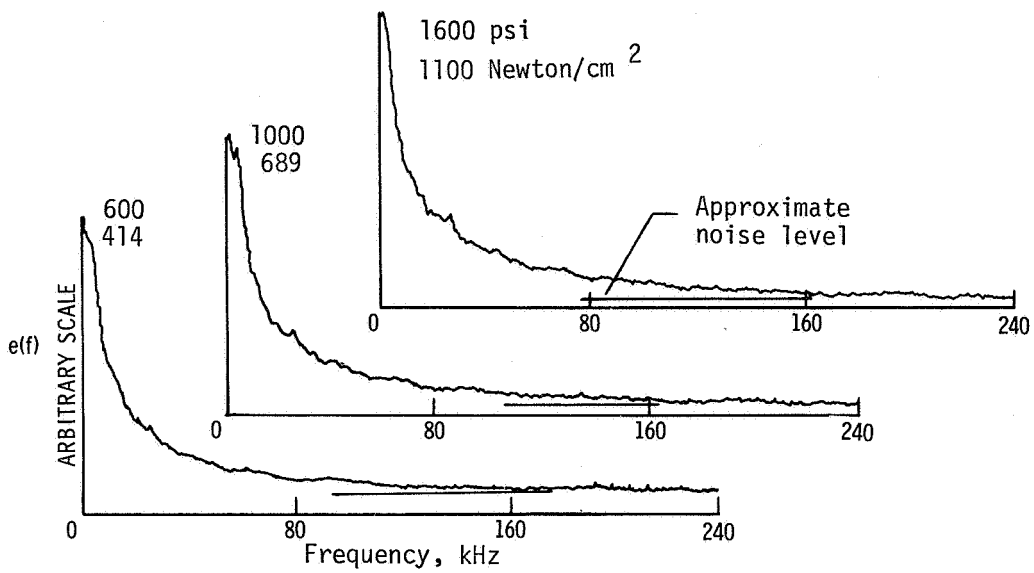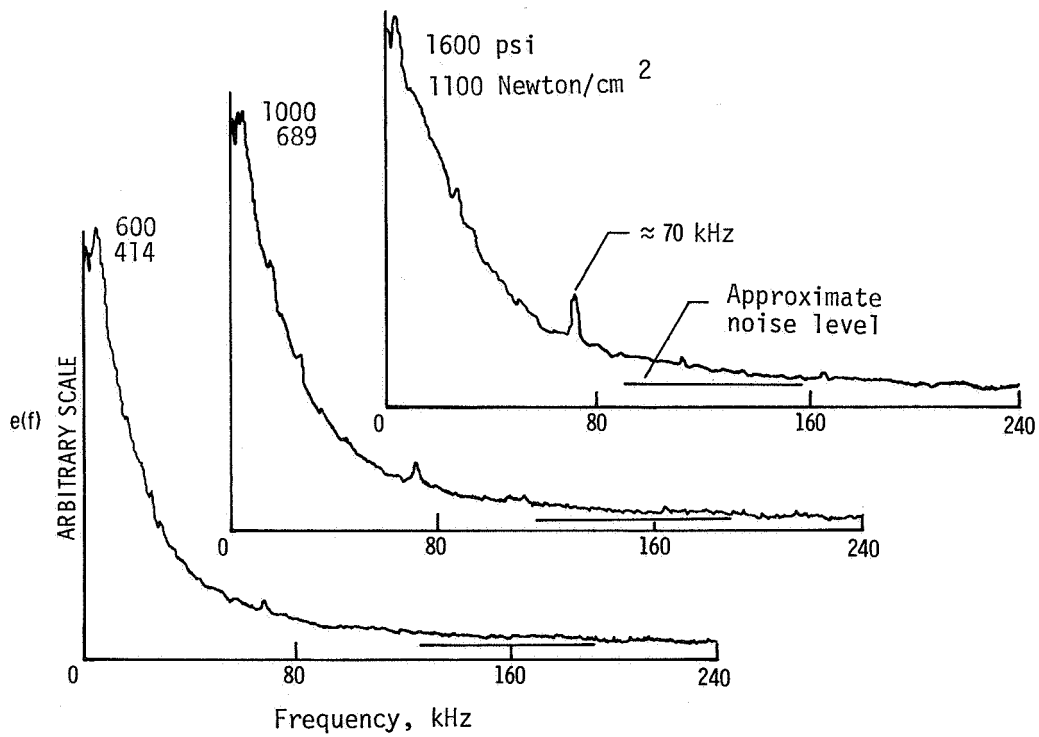

(a) Hot-wire data in 150-cm (60-in.) helium tunnel (Wagner).

Figure 2.- Spectral distributions of wind-tunnel disturbances.
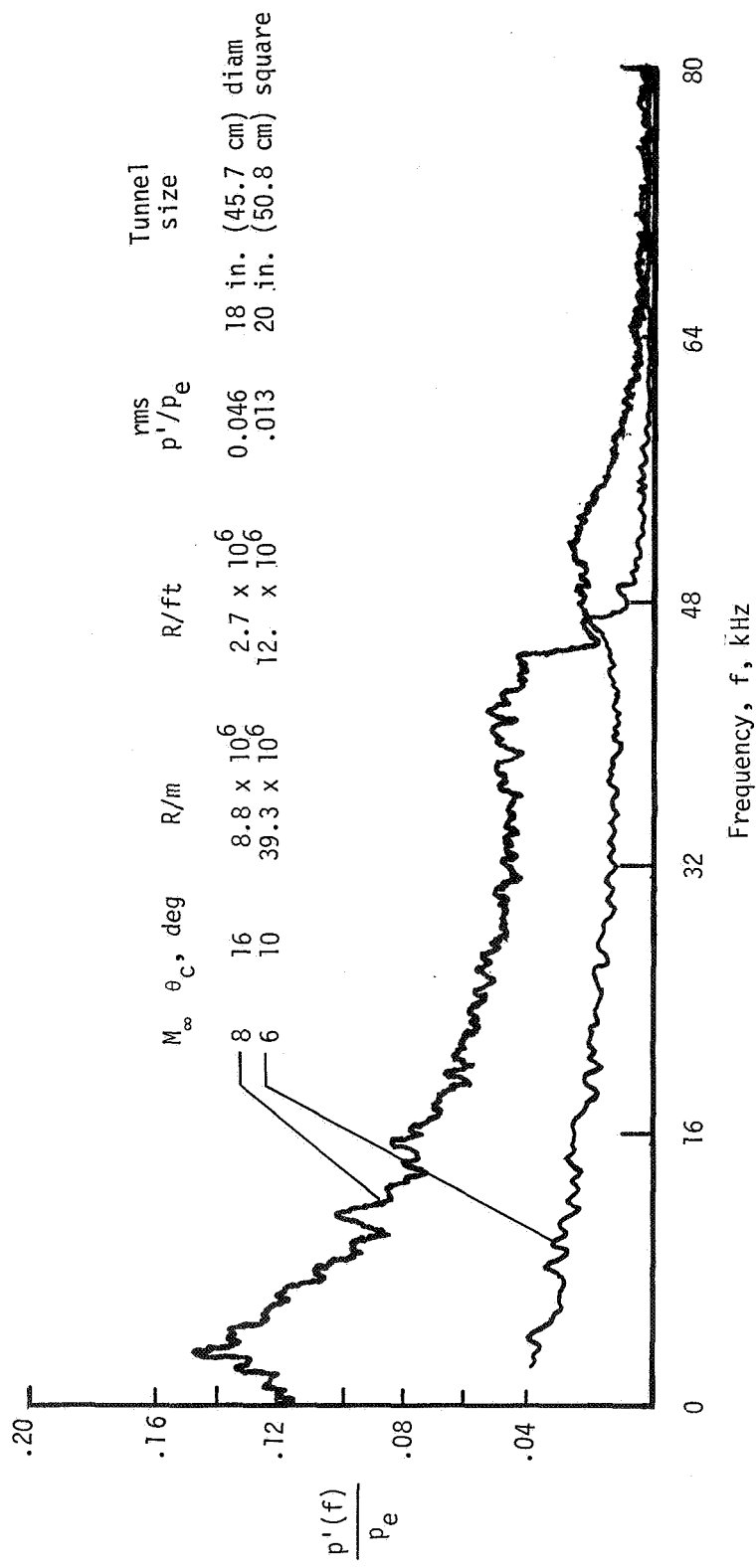
(b) Pressure spectra at cone surface at $M_e = 5$ (ref. 5).

Figure 2.- Concluded.

$$\frac{p'}{p_e(M_\infty)^2}$$

M_∞	M_e	Flow model	Tunnel diam., D^*, or height		
			in.	cm	
3	—	Free stream →	20	50.80	Laufer, stream hot-wire data
4	—		20	50.80	
5	—		20	50.80	
6	5	10° cone →	20	50.80	Stainback, surface pressure data
6	5		12	30.48	
8	5	16° cone	18	45.72	

R_{∞,D^*}

10^6 10^7 3×10^7

.0008
.0006
.0004
.0002
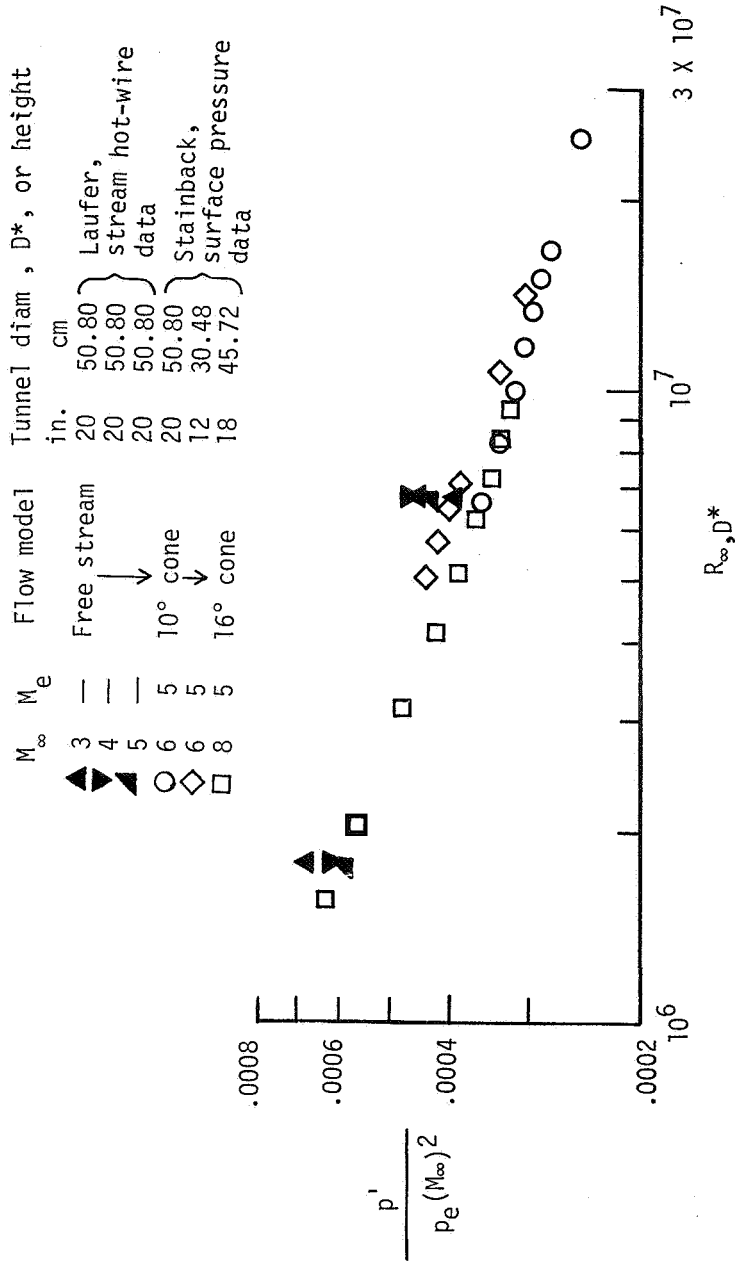
Figure 3.- Comparisons of rms sound measurements from surface pressure transducers and hot wires.

37

θ_c, deg	M_∞	M_e	Diam, in.	cm	Gas	T_w/T_o	
○ 10	6	5	20	50.80	Air	0.6	⎫
□ 16	8		18	45.72		.4	⎬ Stainback
◇ 10	6		12	30.48	↓	.6	⎭
△ 16	20		22	55.88	He	.6	
◁ 16	20	↓	22	55.88		1.0	⎫
⬠ 2.87	20	15.7	22	55.88			⎬ Fischer and
⬡	20	15.6	22	55.88			⎭ Wagner
◇ ↓	18	14.6	60	152.40	↓	↓	

$R_{x,t}$

6×10^7

10^7

10^6

10^6 R/ft 10^7 10^8

3×10^6 10^7 10^8 3×10^8

R/m
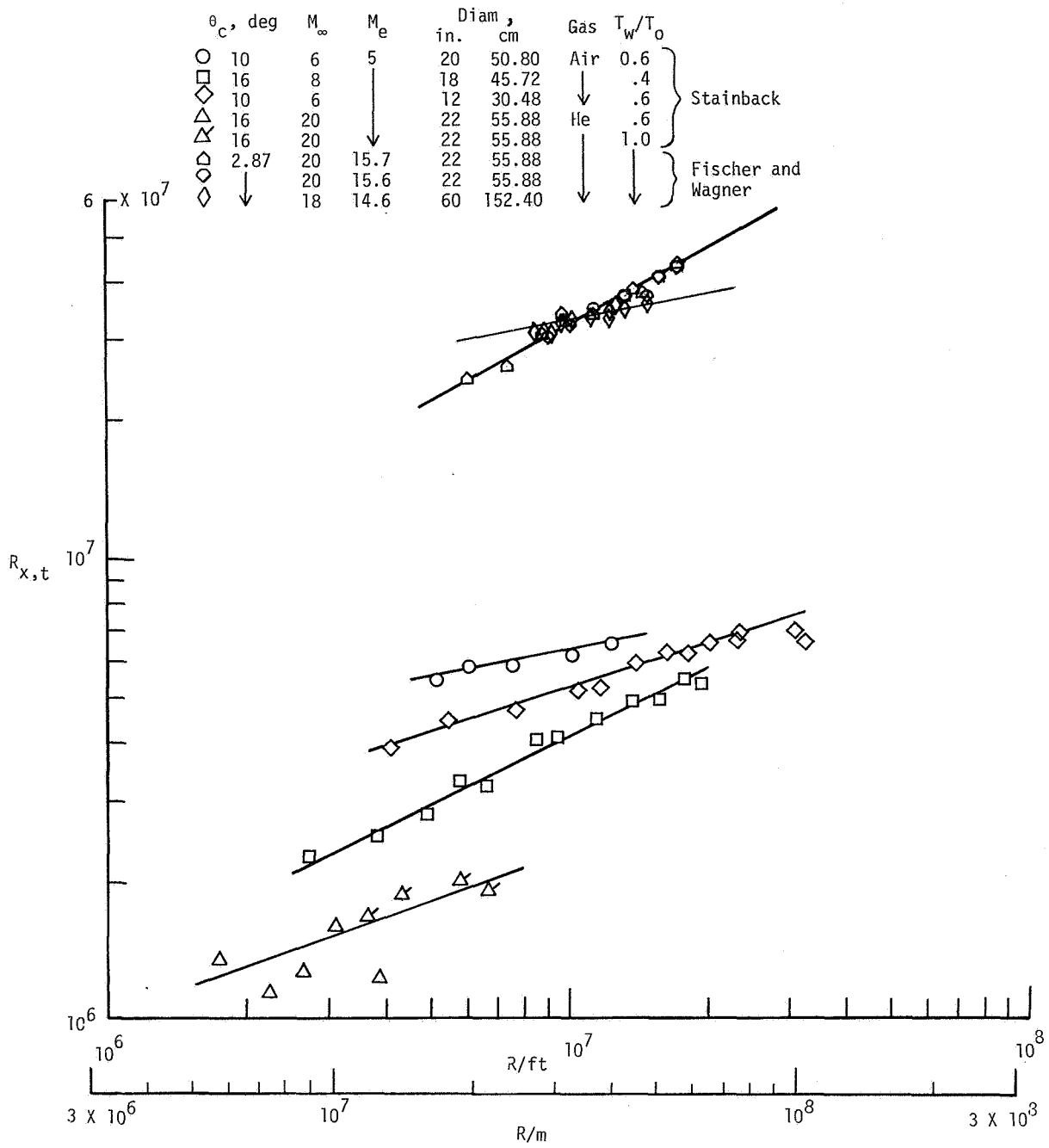
(a) Variation of local transition Reynolds number with local unit Reynolds
number on sharp cones.

Figure 4.- Transition and rms sound measurements in several wind tunnels at
the Langley Research Center.

38
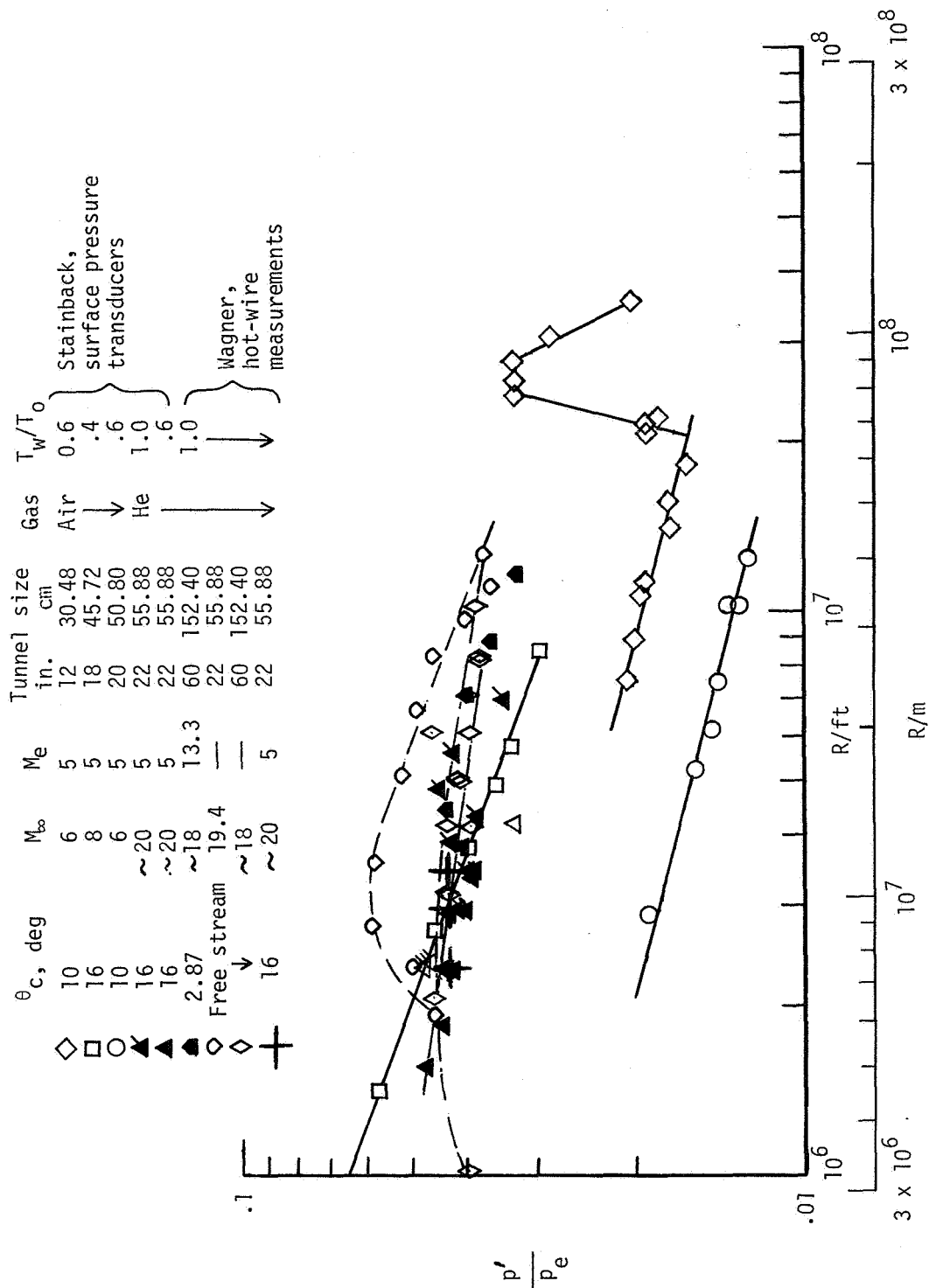
(b) Variation of normalized rms sound pressure with local unit Reynolds number. Hot-wire data from inviscid shock layer of cones and in tunnel free stream.

Figure 4.- Concluded.

39

5×10^7

M_∞	M_e	θ_c, deg	T_w/T_0	Test Gas	Tunnel diam in.	cm	
6	5	10	0.6	Air	20	50.80	
6	5	10	0.6	Air	12	30.48	
8	5	16	0.4	Air	18	45.72	Stainback
20	5	16	1.0	He	22	55.88	
20	5	16	0.6	He	22	55.88	
20	~16.2	2.87	1.0	He	22	55.88	
20	~15.8	2.87	1.0	He	22	55.88	Fischer and Wagner
18	~14.4	2.87	1.0	He	60	152.40	
20	6.8	Wedge	1.0	He	22	55.88	Ref. 8
~0		Flat plate		Air			Refs. 16-18

$R_{x,t}$

10^7

10^6

10^5

$\frac{p'}{p_e}$

$\frac{u'}{u_e}$

10^{-1} 10^{-2} 10^{-3}

$\frac{p'}{p_e}$ or $\frac{u'}{u_e}$
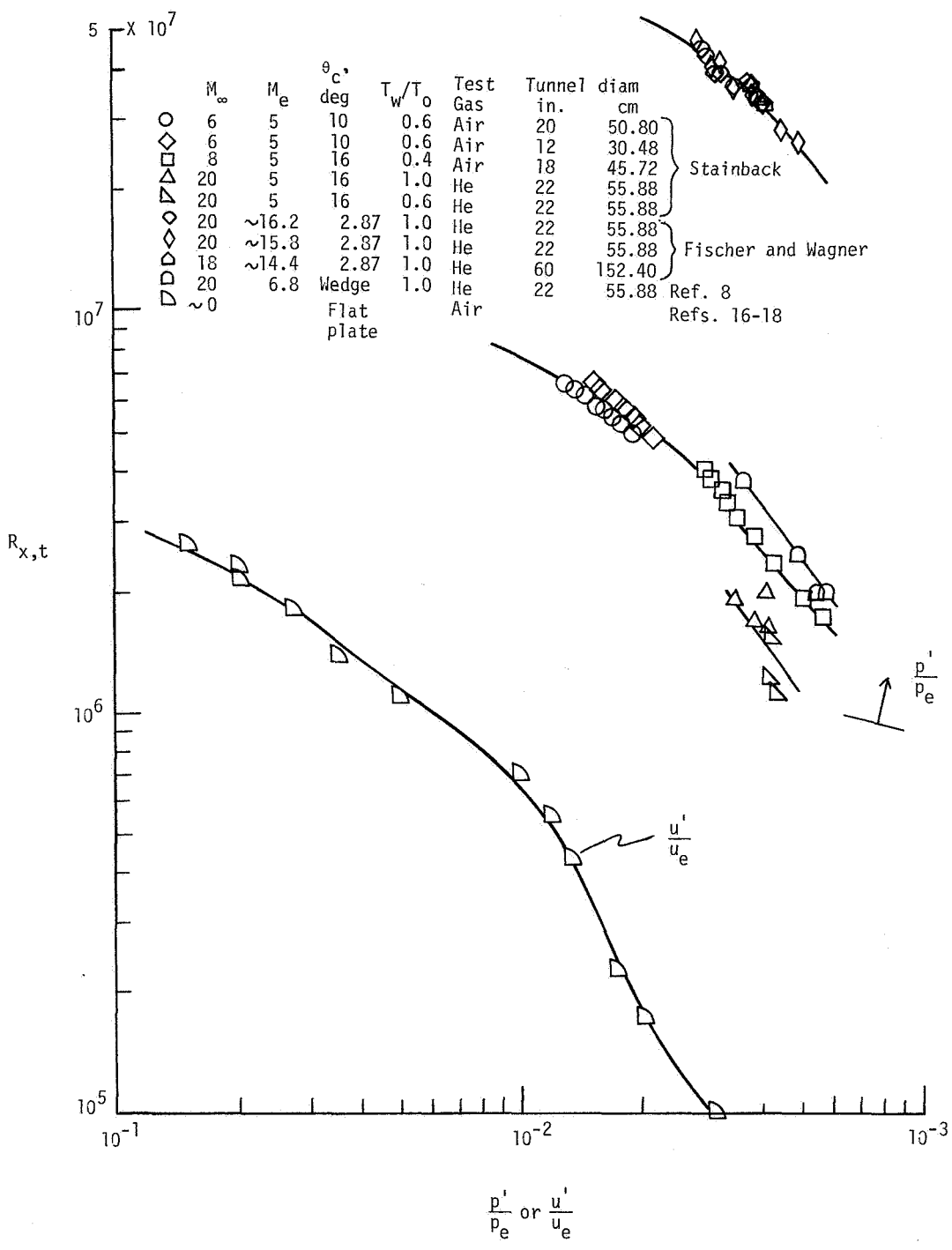
Figure 5.- Correlation of transition Reynolds numbers with rms disturbance levels.

40
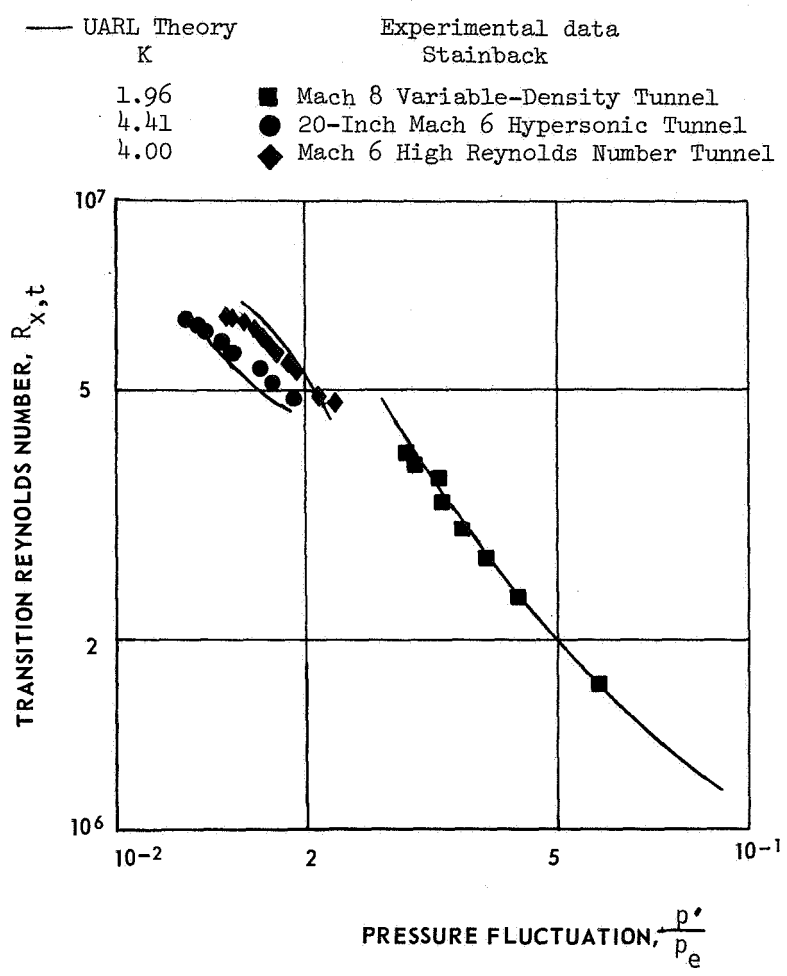
Figure 6.- Comparison of calculated and measured effects of rms sound
pressures on transition location. $M_e = 5$.
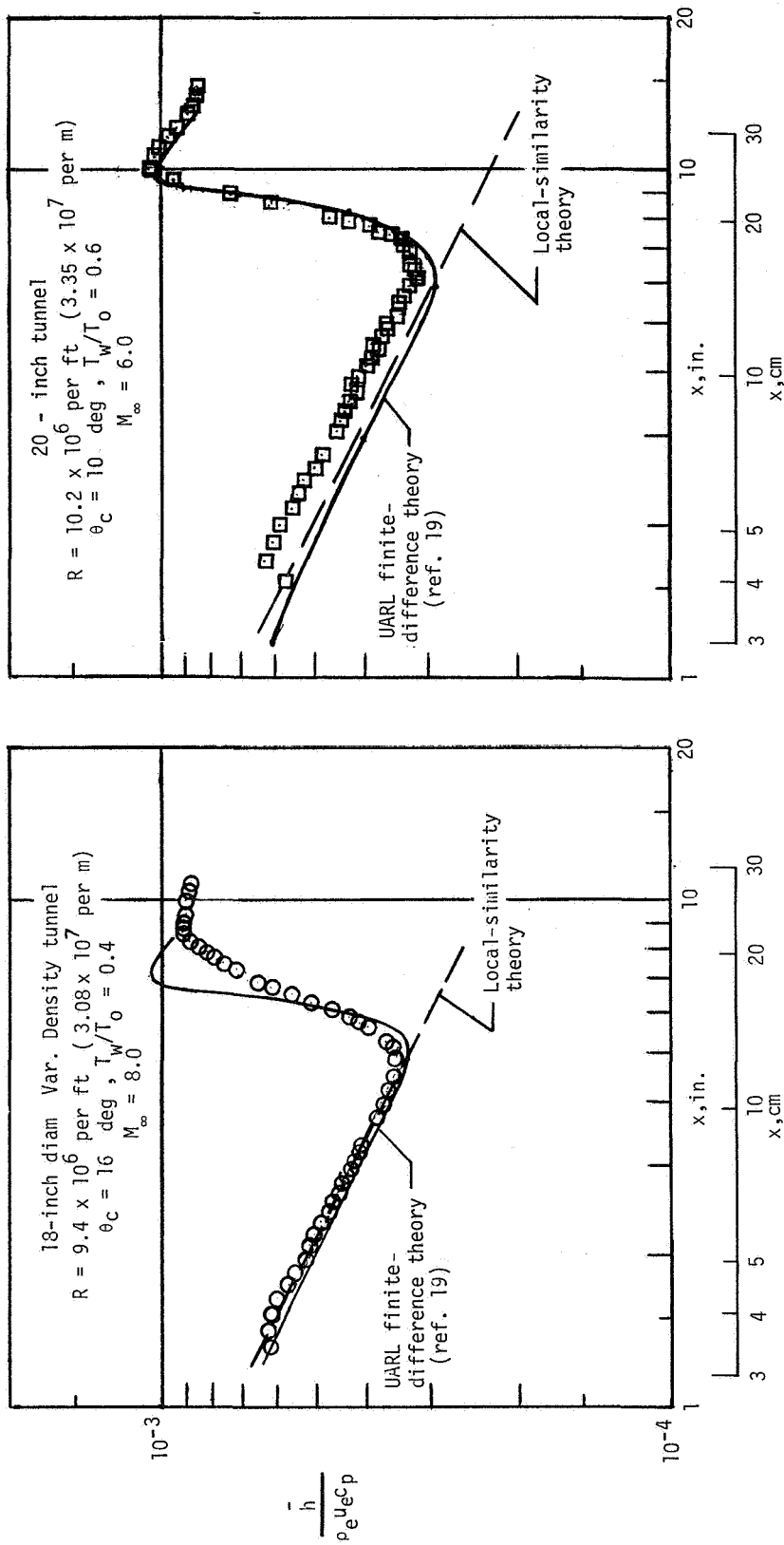
Figure 7.- Experimental and theoretical heat-transfer distributions through transition on sharp cones. $M_e = 5$.
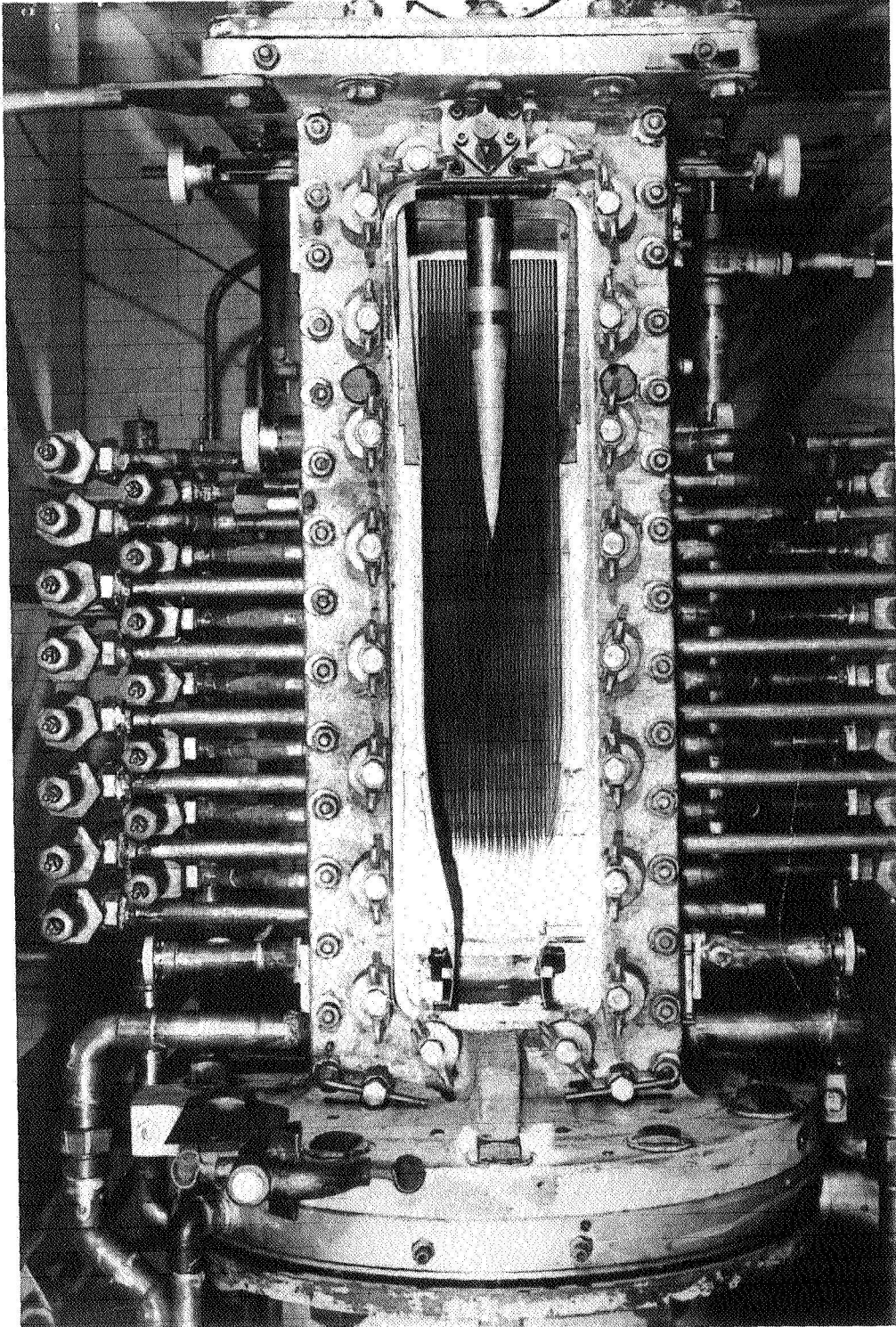
L-72-2423

(a) General view of nozzle and test section.

Figure 8.- Suction laminarization studies on a Mach 2 nozzle at the National Bureau of Standards by Klebanoff and Spangenberg.

43

Mach no. 2

Laminar flow

TURBULENT FLOW

Boundary-layer scoop

Nozzle block (top also)

Suction chamber

(b) Corner suction and boundary-layer scoop.
$p_0 = 1$ atmosphere.

Sidewall detail

$d = .125$ in. (.318 cm)

GAP = .004 - .008 in.
        .01 - .02 (cm)

Nozzle block

To suction

To suction

Laminar flow

MACH NO. 2 →

TURBULENT FLOW

TURBULENT FLOW

in.
28 cm

11

10

20

Distance from throat

$R_{x,t} \approx 3.3 \times 10^6$

(c) Sidewall suction added. $p_0 = 1$ atmosphere.

Figure 8.- Concluded.

44
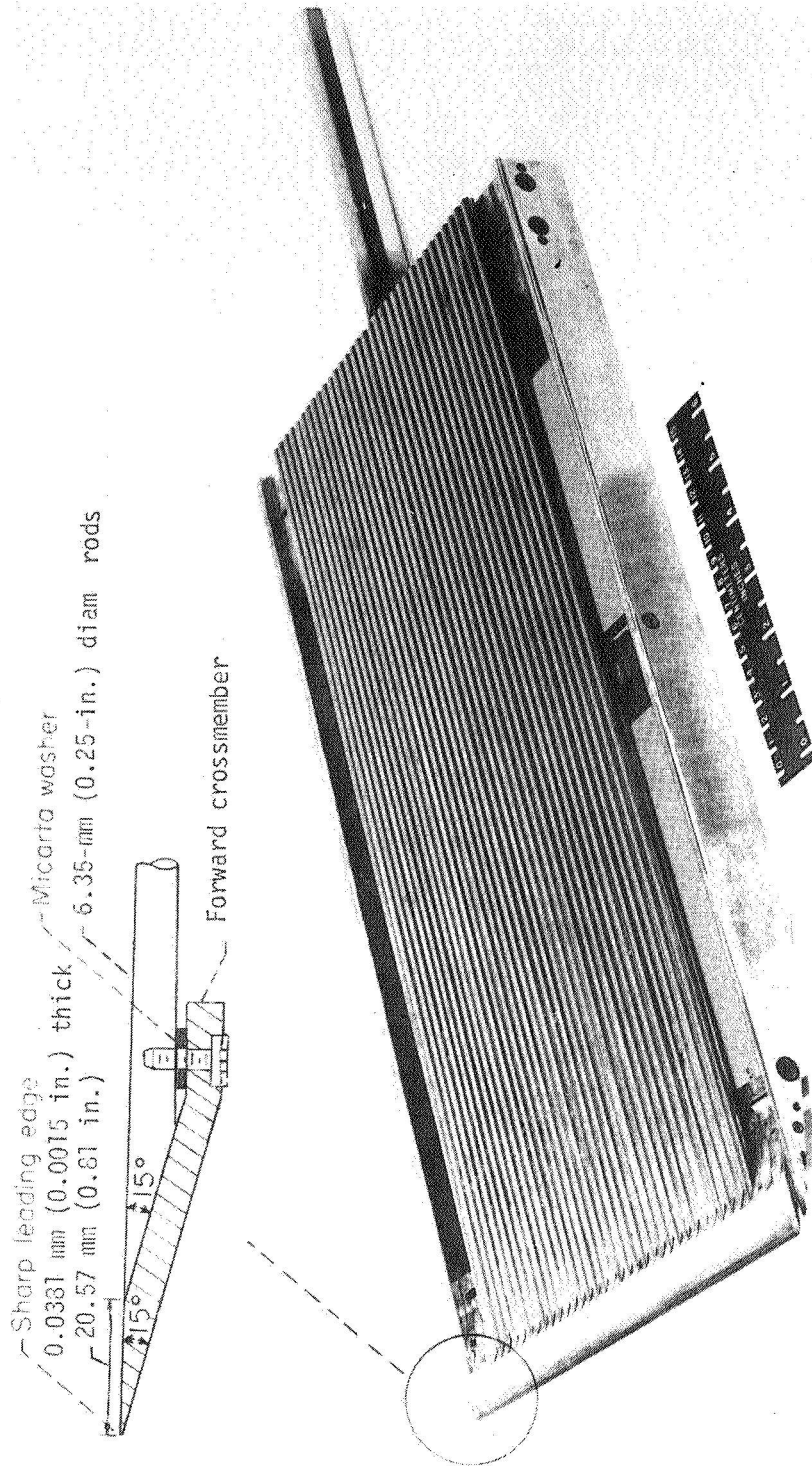
Figure 9.- Photograph of rod suction model. Gaps closed.

45

L-72-2424

Dynamic-pressure transducer
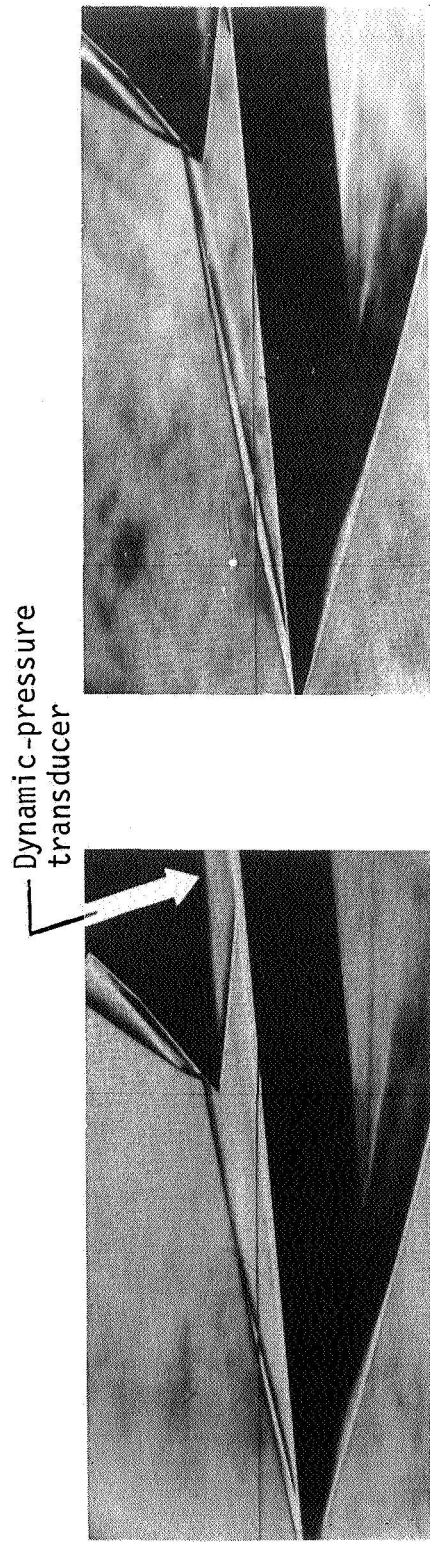
(a) Gaps closed; zero suction; $\dfrac{p'}{p_e} = 0.039$.

(b) Gaps, 1.27 mm (0.050 in.); $\dfrac{(\rho v)_w}{(\rho u)_e} = 0.014$;

$$\dfrac{p'}{p_e} = 0.025.$$

Figure 10.- Schlieren photographs of rod suction model. $\alpha = 5^\circ$; $M_\infty = 8$; $p_0 = 286$ N/cm^2 (415 psia).

46
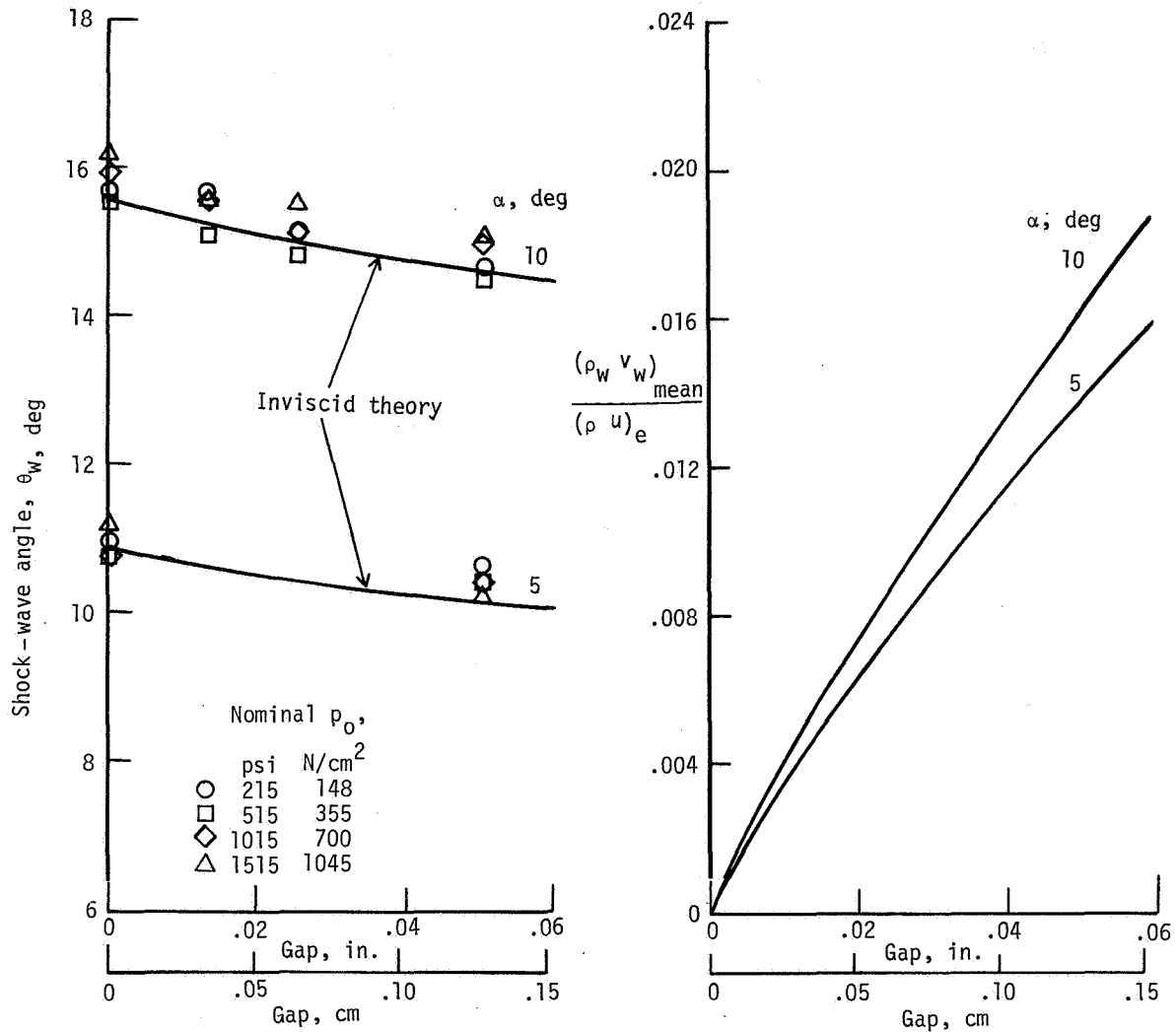
Figure 11.- Shock-wave angle and mean suction mass flow variations with gap width and angle of attack for rod suction model. $M_\infty = 8$.
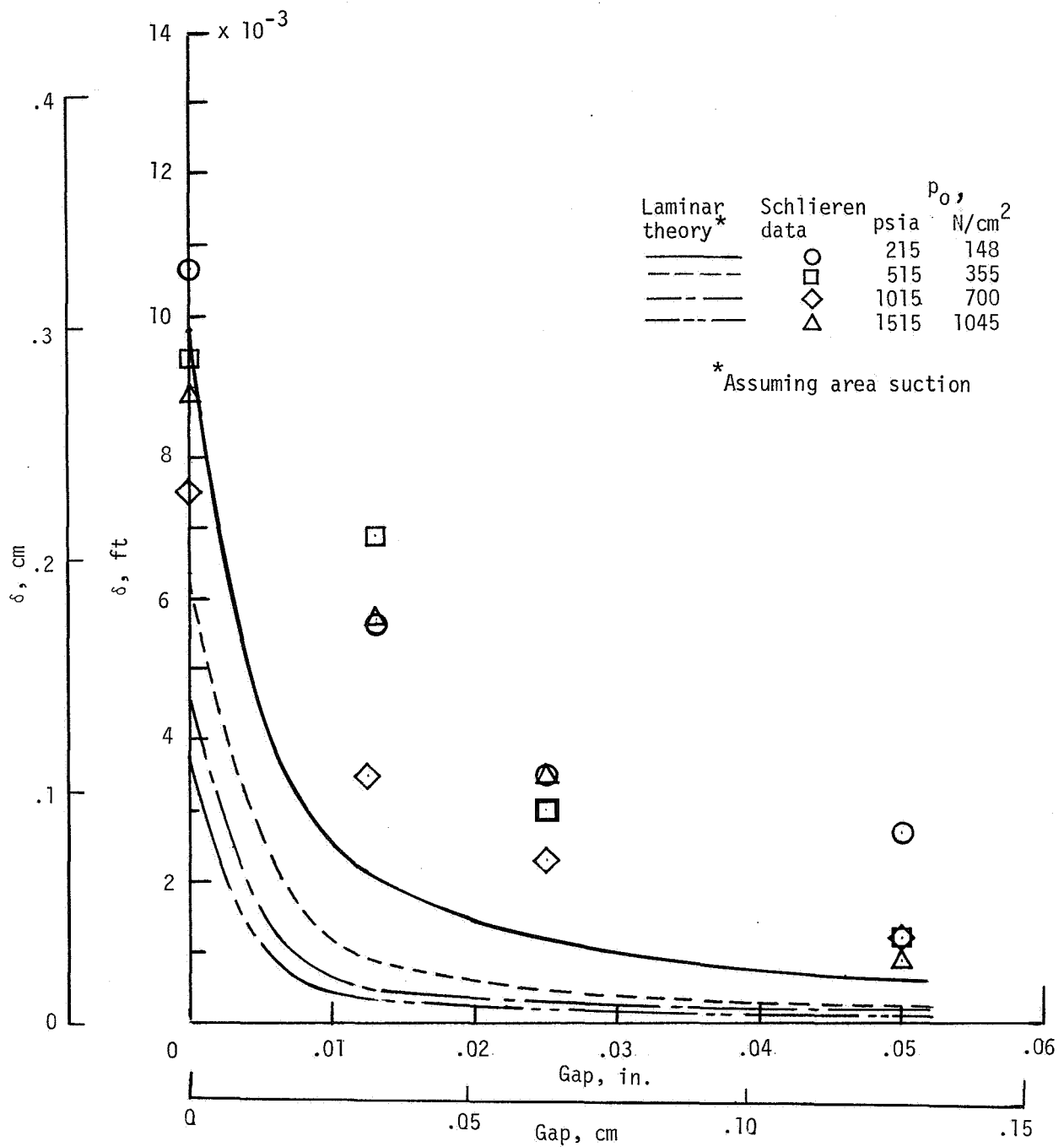
(a) Effect of suction on boundary-layer thickness at x = 0.183 meter (0.6 ft).

Figure 12.- Comparisons of calculated effects of area suction with measured values on rod suction model. $M_\infty = 8$; $\alpha = 10^0$.

48
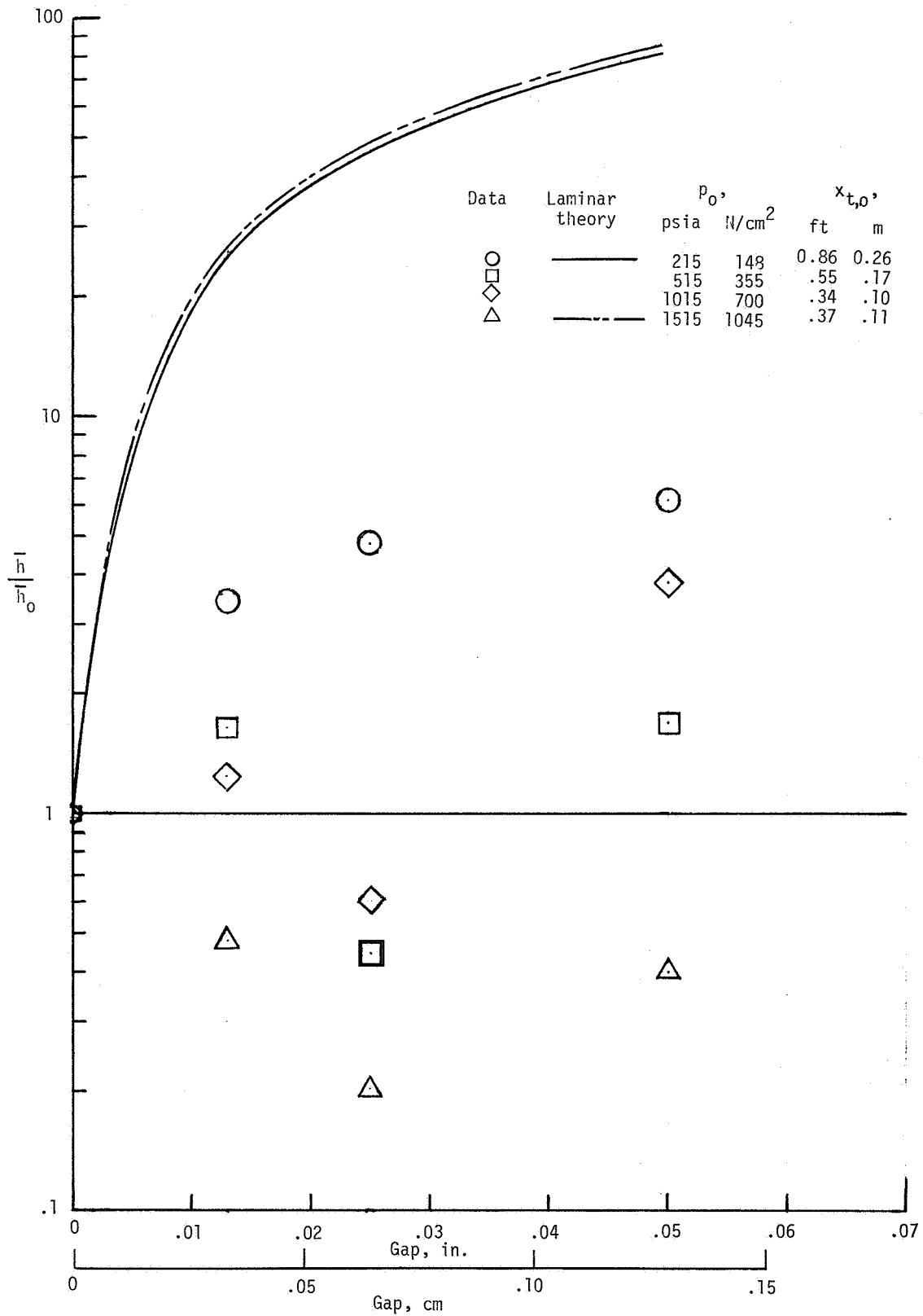
(b) Variation of normalized heat-transfer coefficient at $x_{t,o}$ with gap openings.

Figure 12.- Concluded.

1.6

Rear
support

1.4

Distance to transition location, x_t, m

.4

1.2

Distance to transition location, x_t, ft

.3

.2

Center
support

.1

Rod

Front
support

0

0

End of model

Model	M_e	α,deg	Gap in.	mm	$\dfrac{(\rho v)_w}{(\rho u)_e}$
○ Flat Plate	6.88	4.92	—	—	—
□ Flat Plate	5.74	10.07	—	—	—
◆ Suction	5.76	10.0	0.	0.	0.
	5.83		.013	.33	.005
	5.87		.025	.63	.009
	5.98		.050	1.27	.016
	7.05	5.0	.050	1.27	.014

1.0

.8

.6

.4

.2

10^2
Tunnel stagnation pressure, p_o, psia
10^3
2×10^3

70   100
Tunnel stagnation pressure, p_o, N/cm^2
1000 1200

Figure 13.- Comparison of transition location on a flat plate with that on
rod suction model for different suction rates.

50
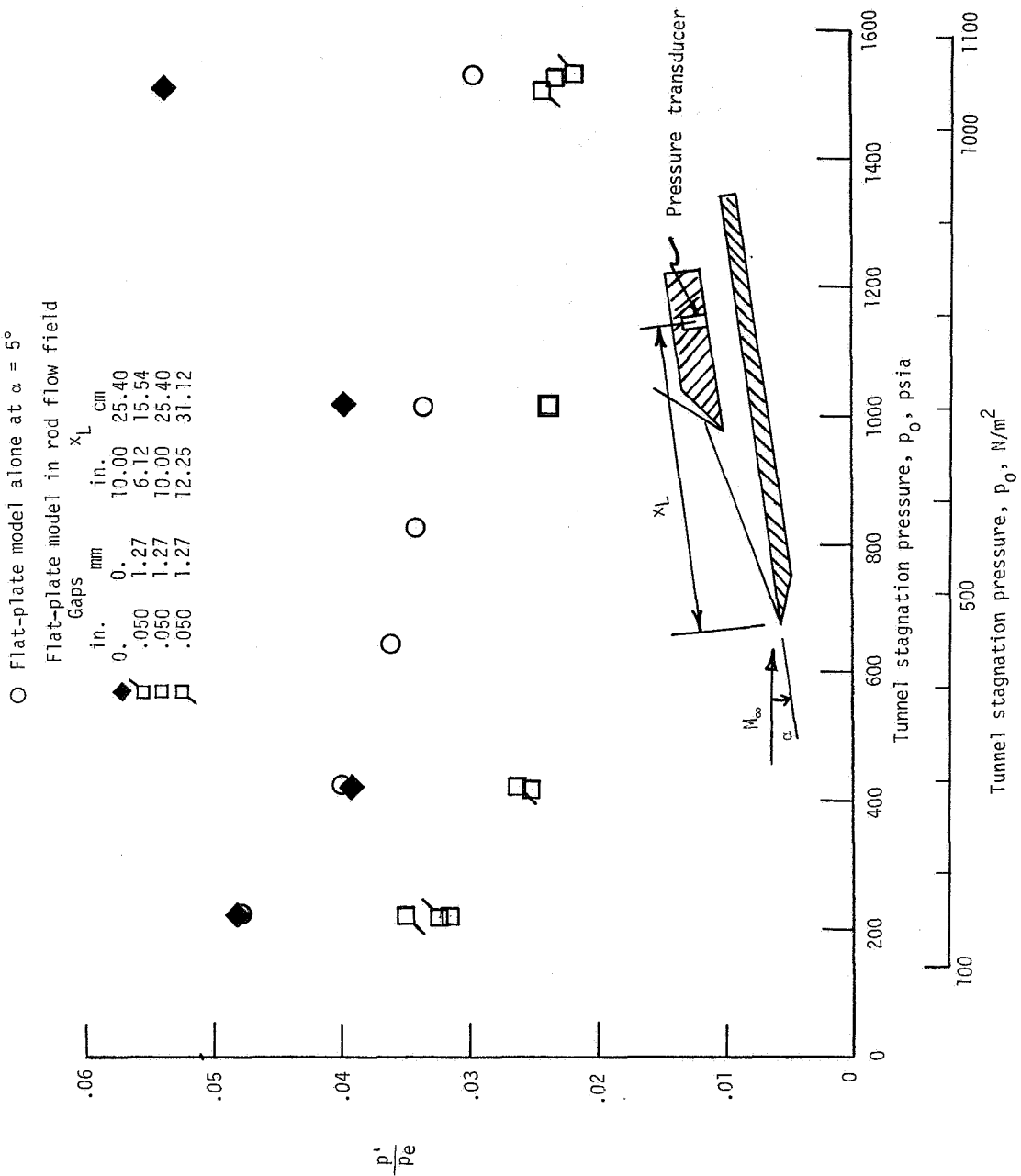
Figure 14.- Sound pressure measurements in flow field of rod suction model at $\alpha = 5^o$ and in equivalent free stream. $M_\infty = 8$.

51
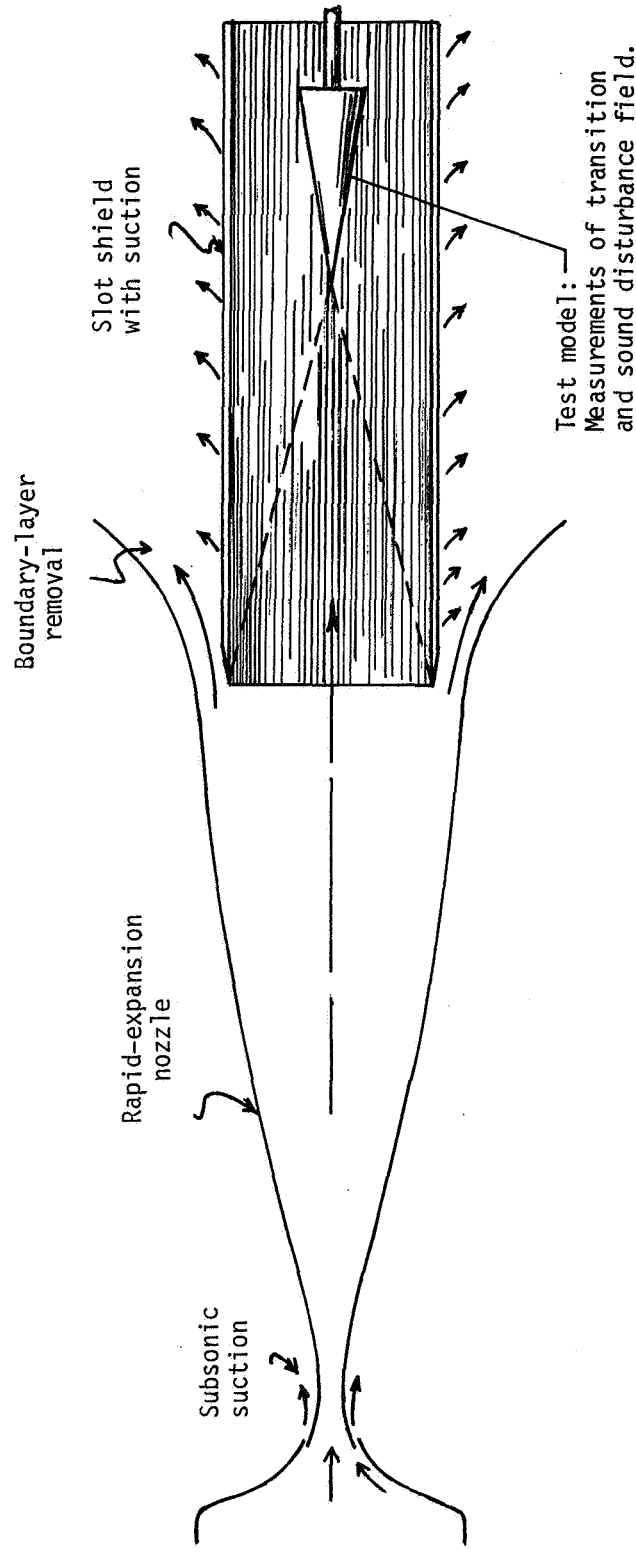
Figure 15.- Application of longitudinal rod suction concept to sound radiation shield in a hypersonic wind tunnel.

Slot shield
with suction

Boundary-layer
removal

Rapid-expansion
nozzle

Subsonic
suction

Test model:
Measurements of transition
and sound disturbance field.
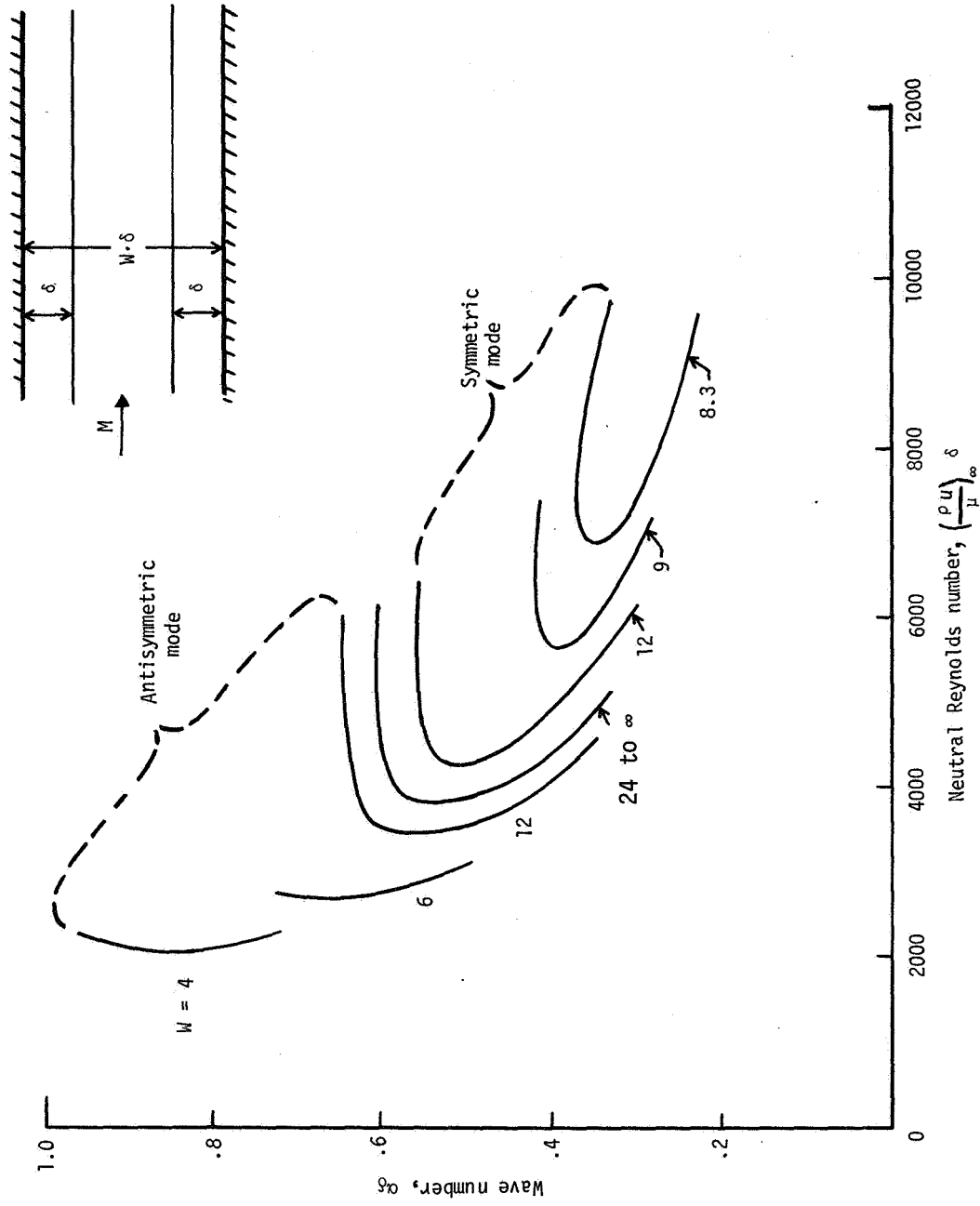
Figure 16.- Linear stability analysis showing effect of channel width with equal boundary-layer thicknesses at M = 2.2.

Figure 17.- Typical results for minimum σ_x correlation of transition on sharp cones at $\alpha = 0^{\circ}$. The symbol + denotes blunt-cone data.

54
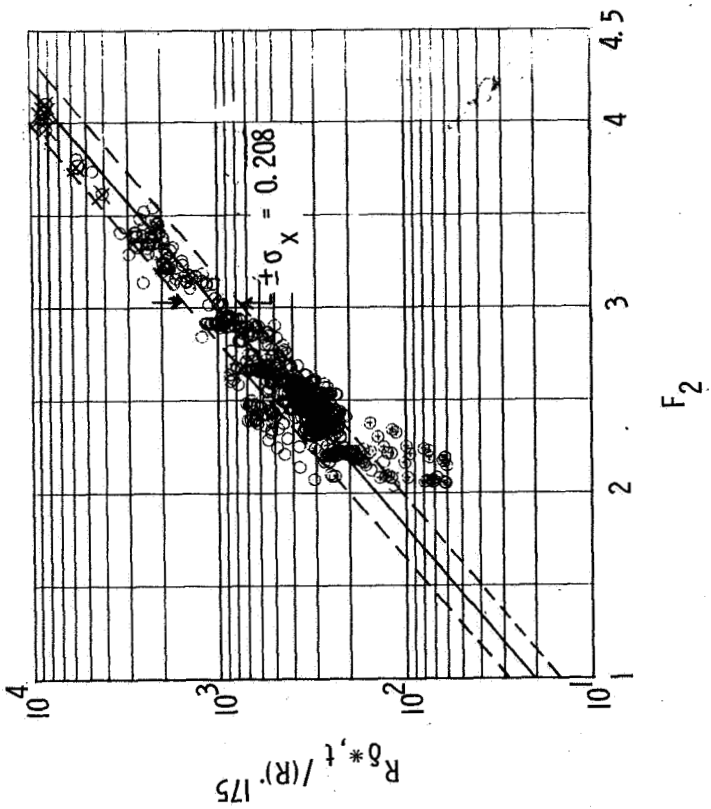
(a) Distribution of flight data with F_1 parameter.   (b) Distribution of all data with F_2 parameter.

Figure 18.- Comparison of Reentry F flight data with other data in terms of typical correlation parameters. The symbol + denotes blunt-cone data.
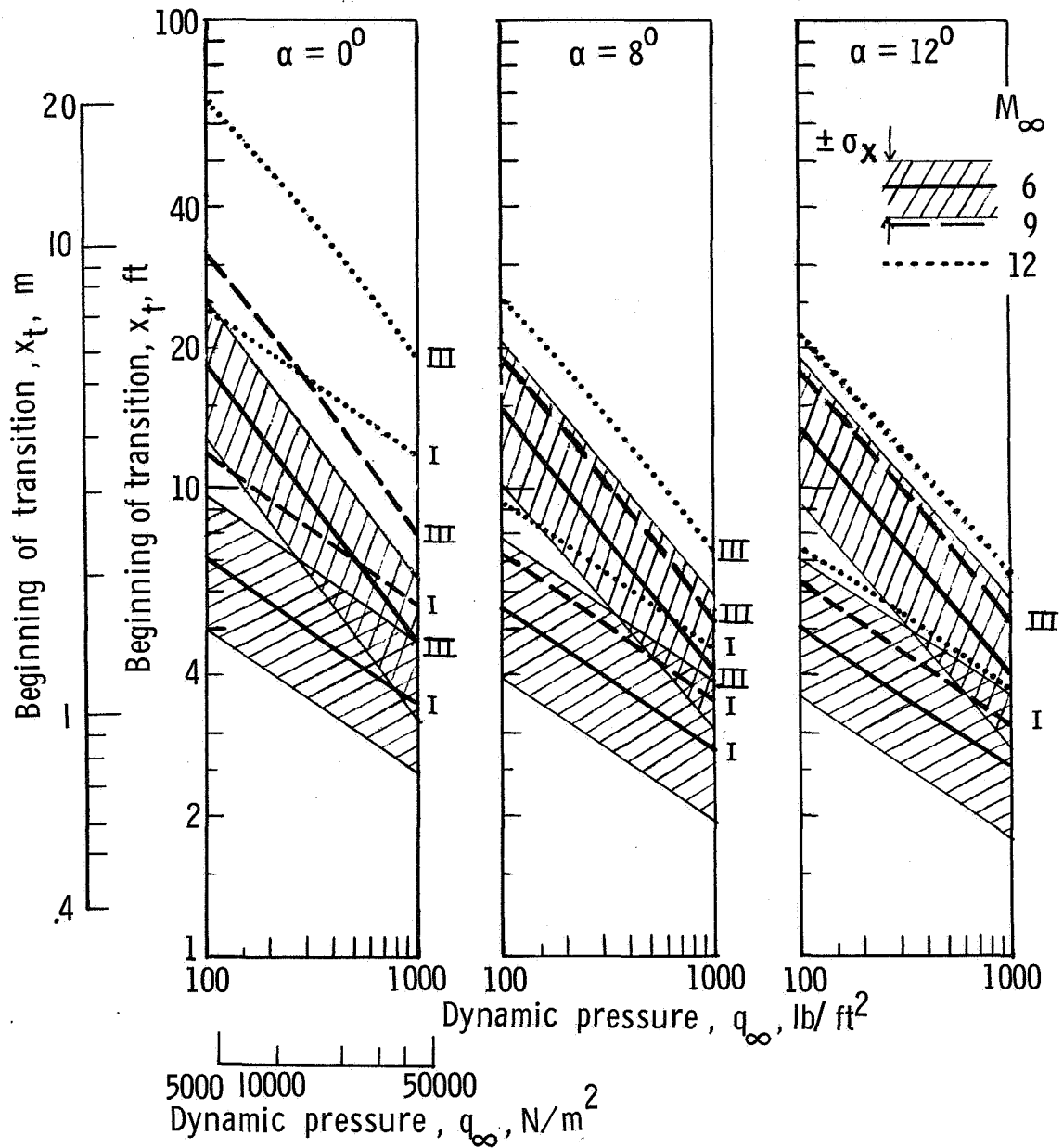
(a) Variation of transition distance x_t with free-stream dynamic pressure q_∞.

Figure 19.- Application of sharp-cone correlations to transition predictions on a flat plate for hypersonic flight conditions. Roman numerals refer to transition parameter used. (See eqs. (4) and table II(a).)

α, deg	0			8			12		
M_∞	6	9	12	6	9	12	6	9	12
M_e	6	9	12	4.91	6.76	8.20	4.37	5.72	6.61
q_∞, lb/ft^2 (N/m^2)	R_∞/ft x 10^{-6} (R_∞/m x 10^{-6}) T_w, °R (°K)			R_∞/ft x 10^{-6} (R_∞/m x 10^{-6}) T_w, °R (°K)			R_∞/ft x 10^{-6} (R_∞/m x 10^{-6}) T_w, °R (°K)		
100 (4788)	0.0912(0.299) 1000(556)	0.0575(0.189) 1000(556)	0.0438(0.144) 1000(556)	0.142(0.466) 1150(639)	0.102(0.335) 1350(750)	0.0820(0.269) 1450(806)	0.156(0.512) 950(528)	0.106(0.348) 1500(833)	0.0793(0.260) 1650(917)
200 (9576)	0.197(0.646) 1050(583)	0.120(0.394) 1100(611)	0.0862(0.283) 1150(639)	0.305(1.000) 1250(694)	0.212(0.695) 1450(806)	0.162(0.531) 1600(889)	0.336(1.102) 1100(611)	0.222(0.728) 1650(917)	0.156(0.512) 1850(1028)
500 (23940)	0.539(1.768) 1200(667)	0.332(1.089) 1250(694)	0.234(0.768) 1250(694)	0.831(2.726) 1400(778)	0.582(1.909) 1650(917)	0.436(1.430) 1800(1000)	0.913(2.995) 1350(750)	0.605(1.985) 1800(1000)	0.420(1.378) 2000(1111)
1000 (47880)	1.11(3.641) 1300(722)	0.714(2.342) 1350(750)	0.504(1.653) 1400(778)	1.70(5.576) 1500(833)	1.25(4.100) 1800(1000)	0.932(3.057) 2000(1111)	1.87(6.134) 1500(833)	1.29(4.231) 1950(1084)	0.895(2.936) 2250(1250)

(b) Free-stream and local conditions.

Figure 19.- Concluded.
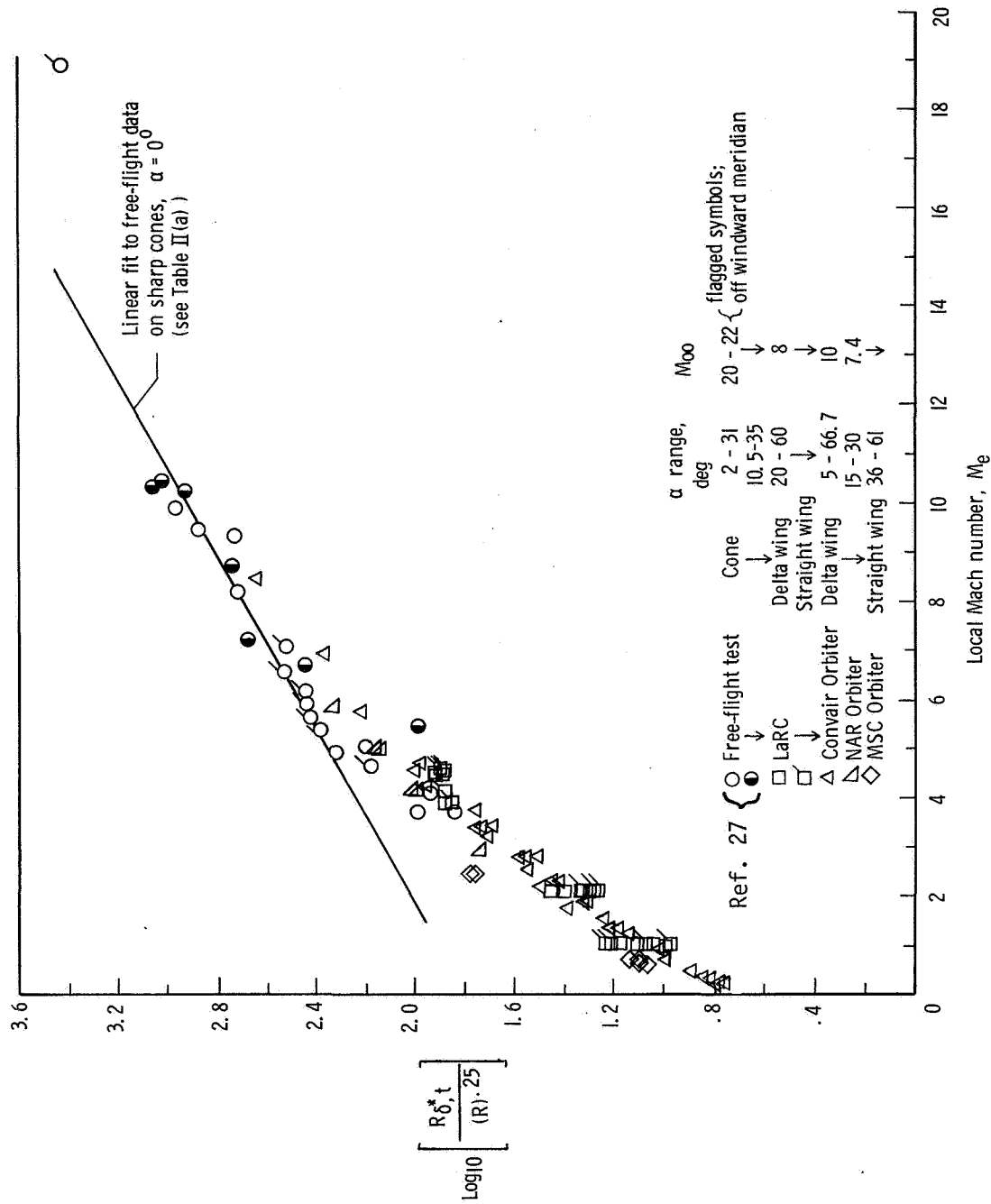
Figure 20.- Application of transition correlations for cones at $\alpha = 0^o$ to various shapes at angle of attack. (See ref. 26.)
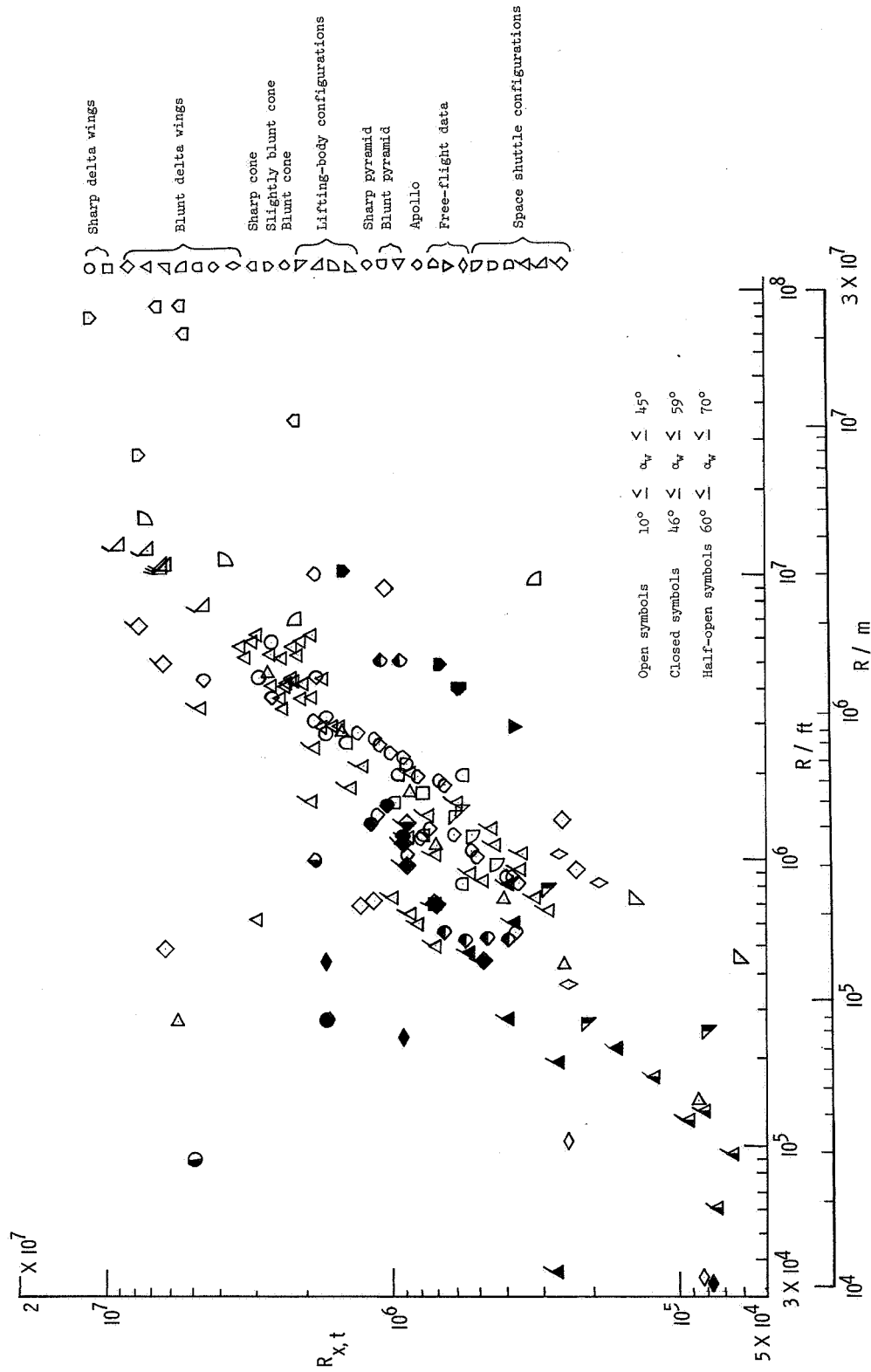
(a) Transition Reynolds number as a function of local unit Reynolds number.

Figure 21.- Summary of transition data on windward symmetry line of various shapes for $\alpha_w \gtrsim 10^o$.

59
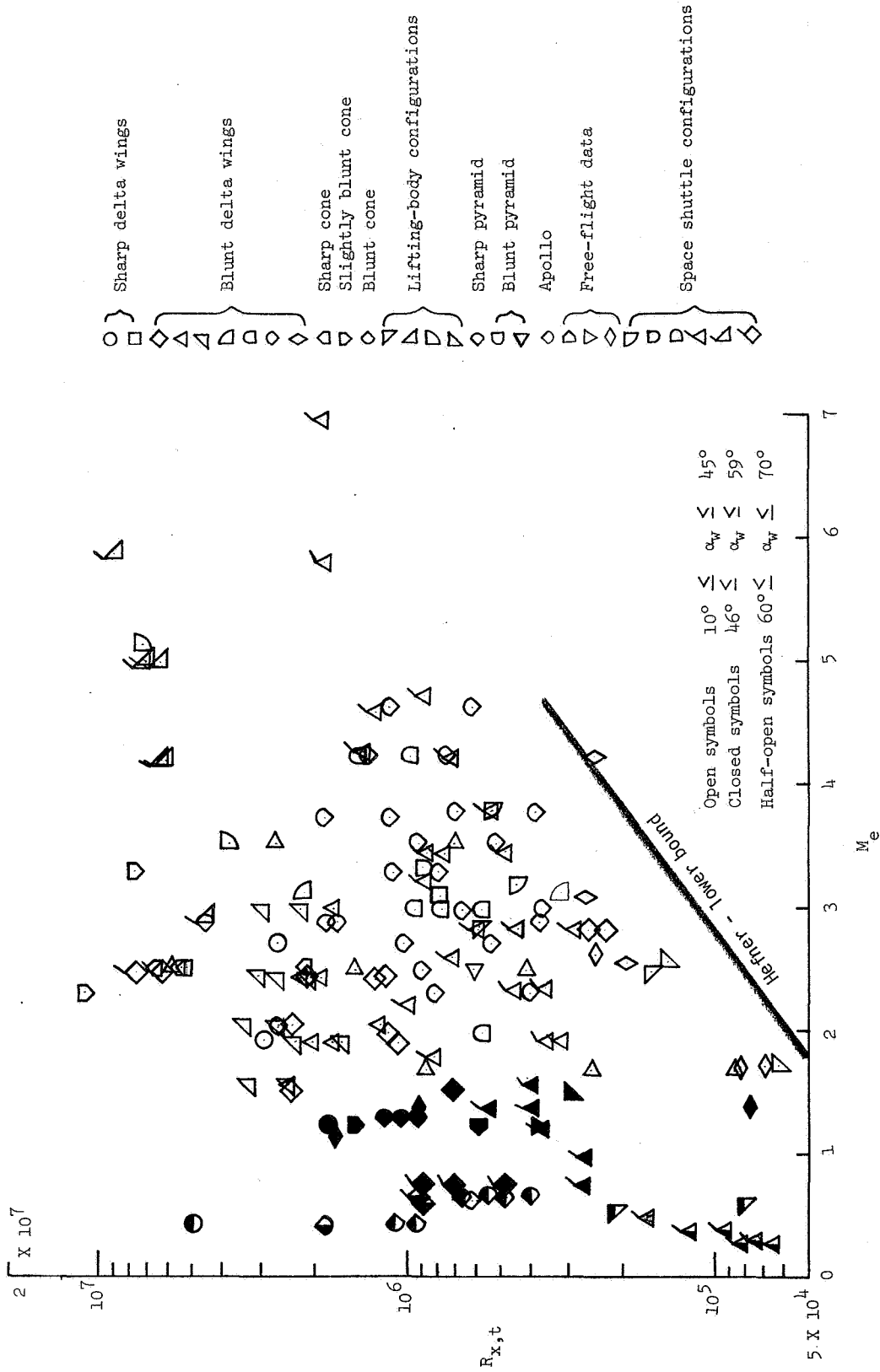
(b) Transition Reynolds number as a function of local Mach number.

Figure 21.- Concluded.

60

SOURCE	r, cm	METHOD OF DETECTION	R_∞/cm
○ PRESENT	.0102	HEAT TRANSFER	0.47×10^6
□ REF. 30	.0076	FIXED SURFACE PITOT PROBE	VARIABLE

$$\theta_c = 2.87^0, \quad T_w/T_{t,\infty} \approx 1.0$$
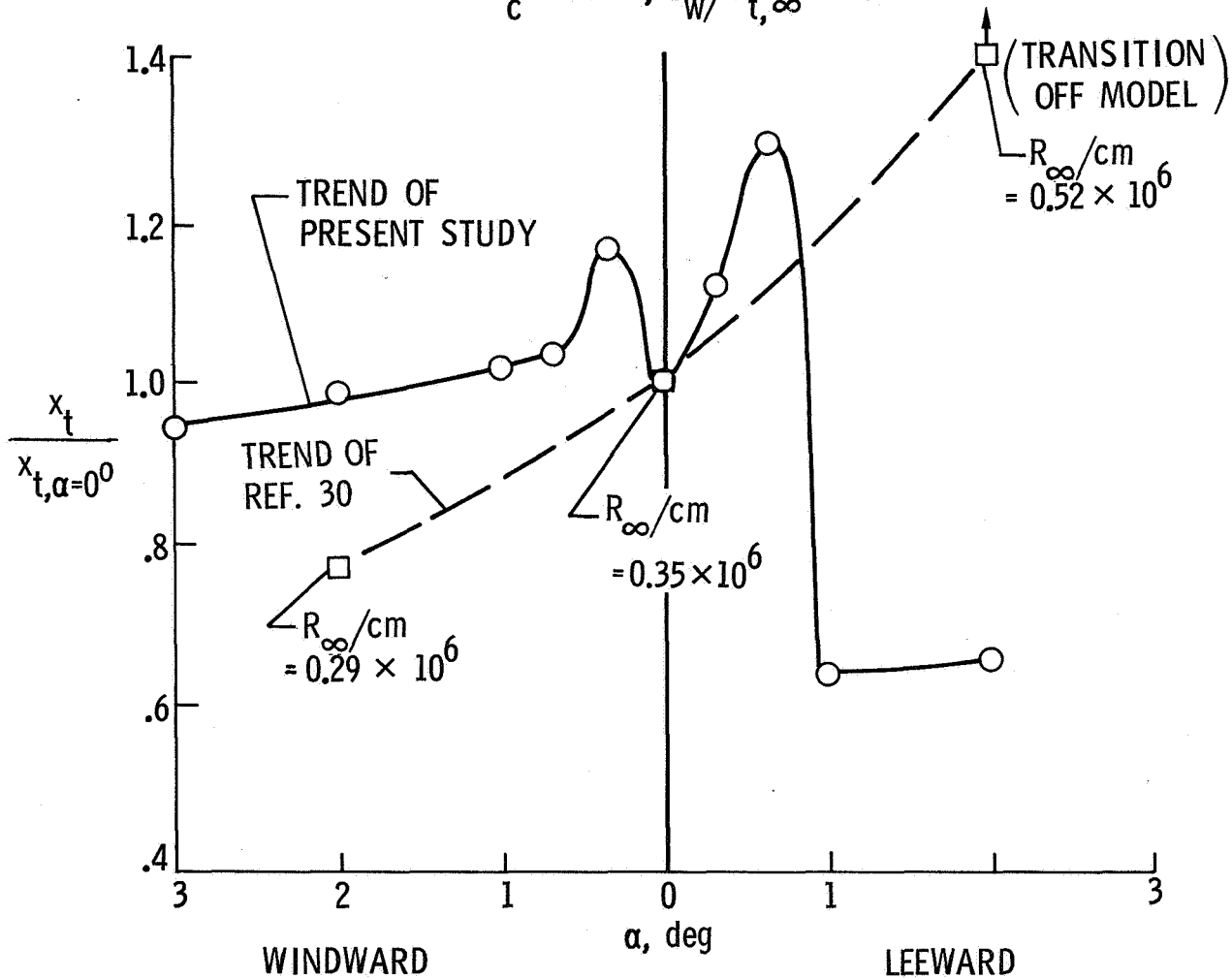
(a) Effect of measurement techniques.

Figure 22.- Transition on slightly blunted cones at small angle of attack.

$$\left(R_\infty/cm \times 30.48 = R_\infty/ft.\right)$$

61

Beginning of transition
○ Heating-rate distribution
□ Temperature history
△ Heating-rate history

10 km

10 x 10³ ft

Relative altitude

1 ft

1 m

Relative axial length
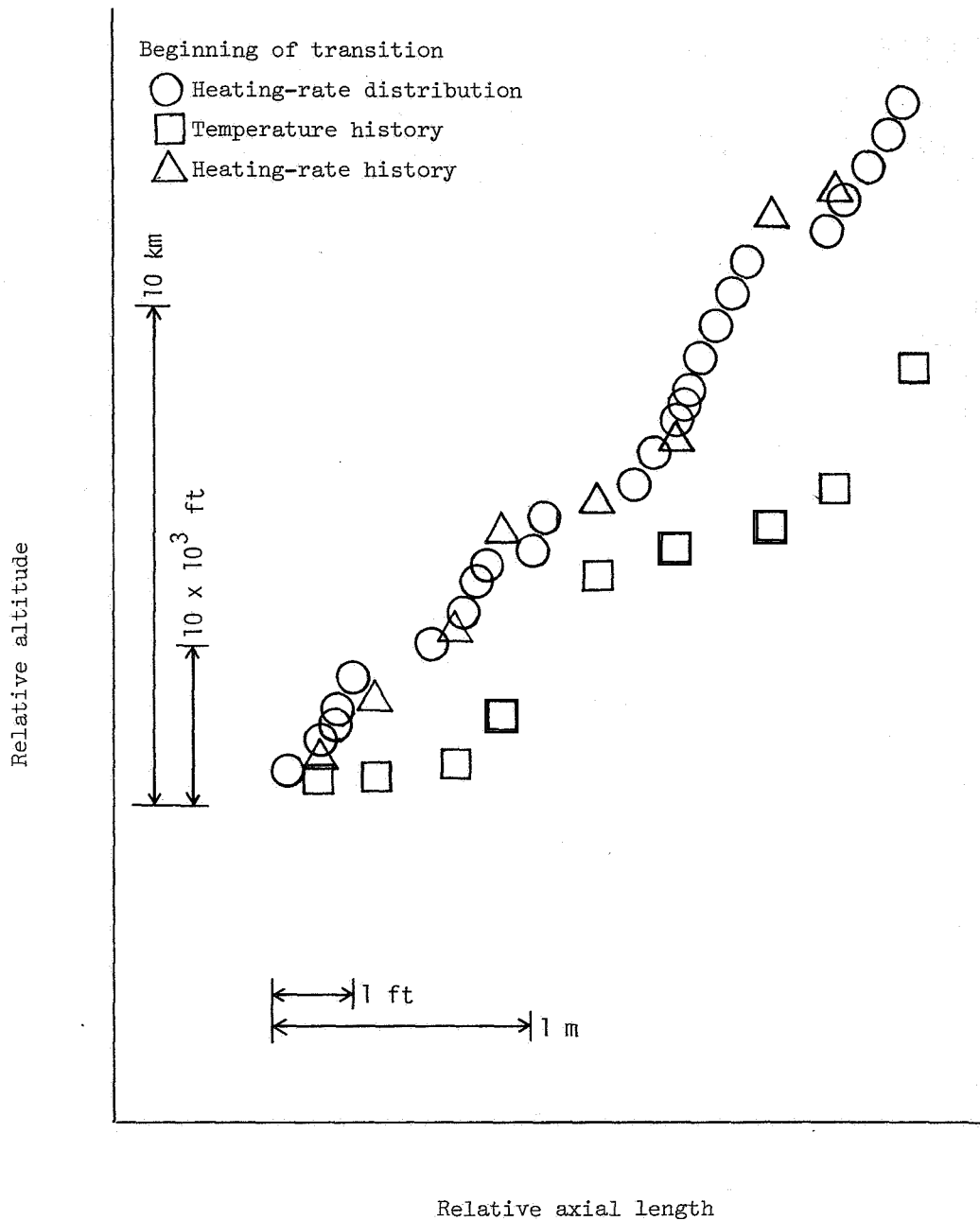
(b) Comparison of transition locations from heating-rate histories, temperature histories, and heating-rate distributions for Reentry F flight test.

Figure 22.- Continued.
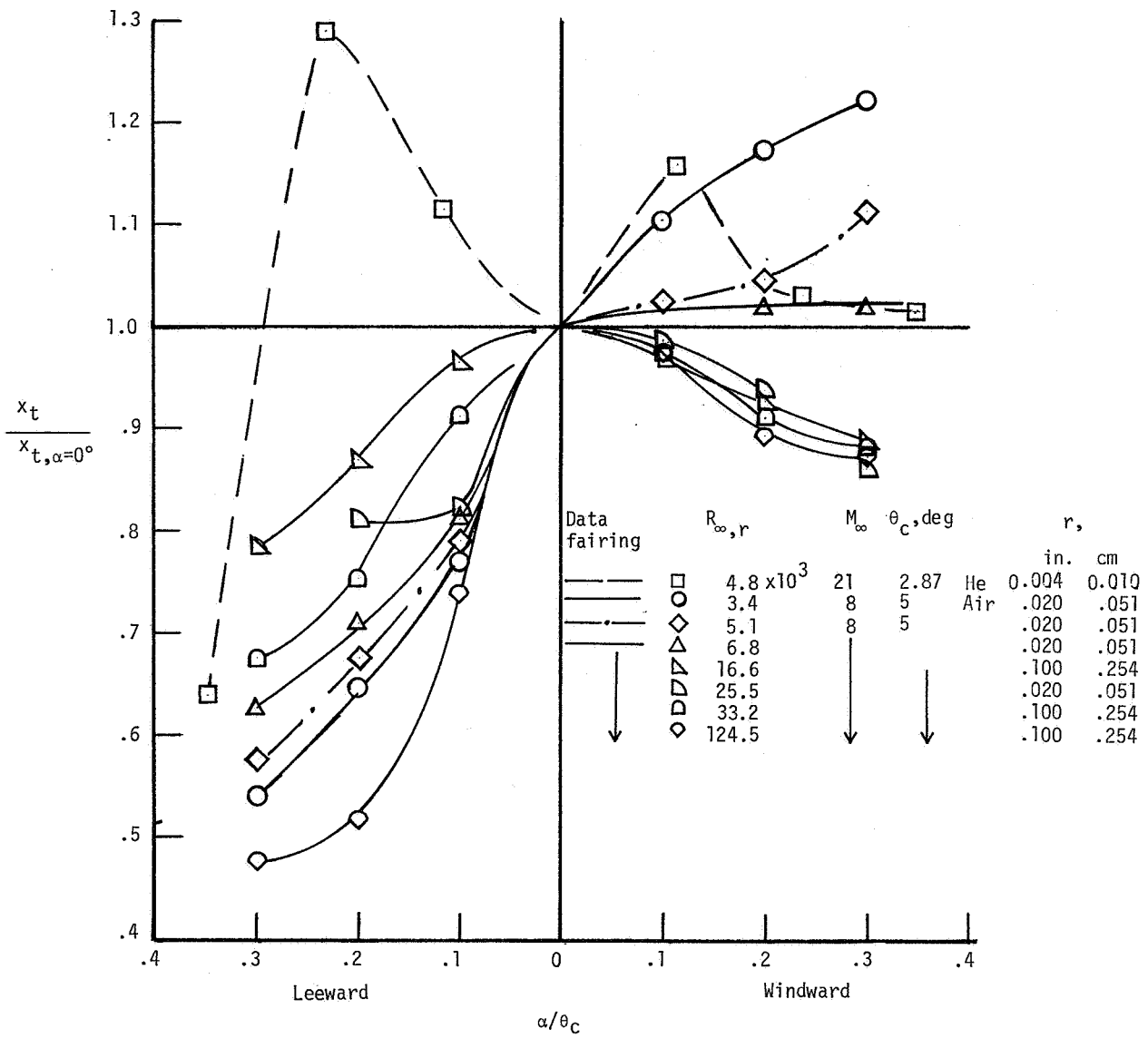
(c) Effect of bluntness Reynolds number.

Figure 22.- Concluded.
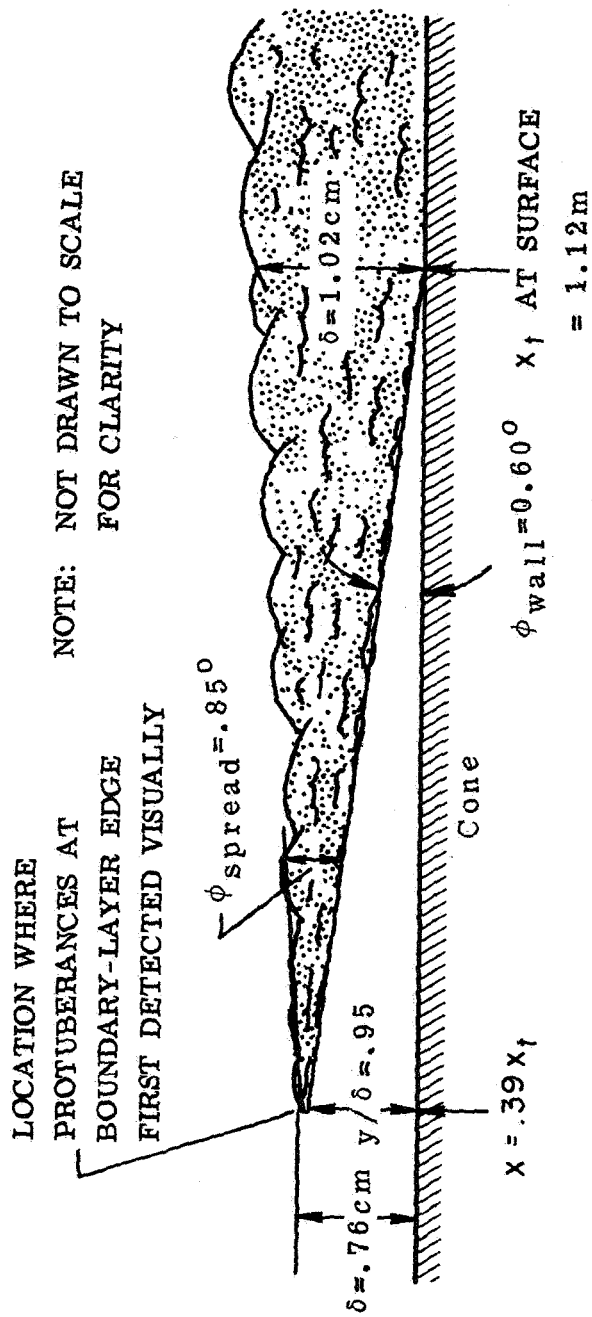
Figure 23.- Spread of mean turbulence in a hypersonic boundary layer based on schlieren photographs and surface heat transfer. $R = 27.9 \times 10^6$ per meter $(8.5 \times 10^6$ per foot$)$; $M_e = 13.6$.
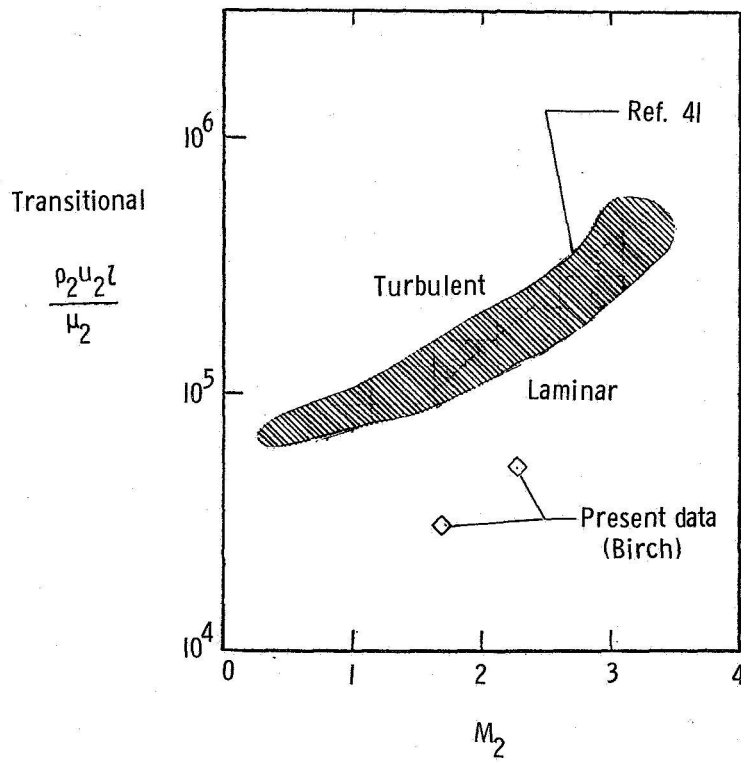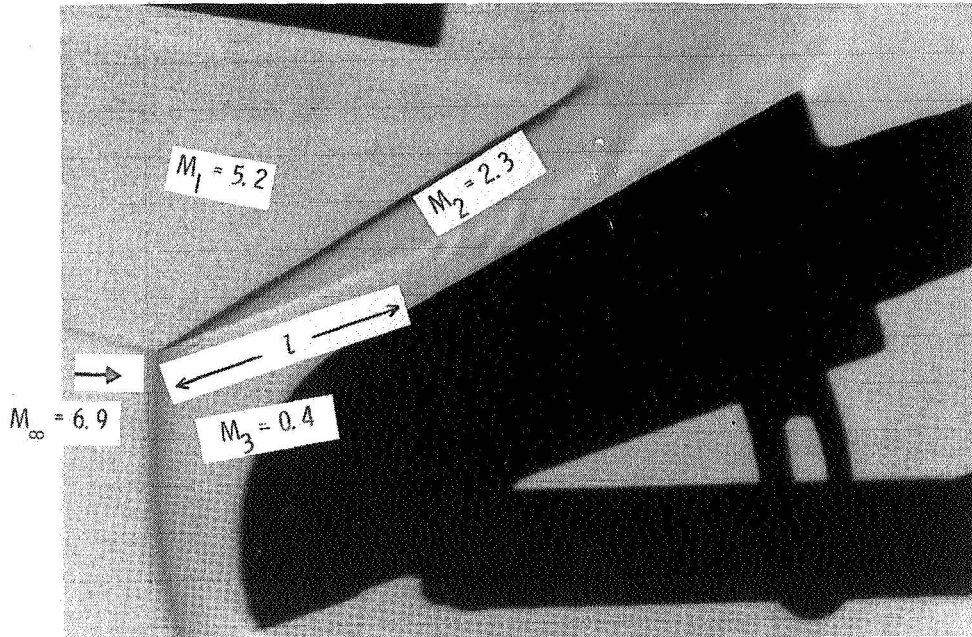
Figure 24.- Transitional flow in free shear layers.

L-72-2425

*"The aeronautical and space activities of the United States shall be
conducted so as to contribute . . . to the expansion of human knowl-
edge of phenomena in the atmosphere and space. The Administration
shall provide for the widest practicable and appropriate dissemination
of information concerning its activities and the results thereof."*

— NATIONAL AERONAUTICS AND SPACE ACT OF 1958

NASA SCIENTIFIC AND TECHNICAL PUBLICATIONS

TECHNICAL REPORTS: Scientific and
technical information considered important,
complete, and a lasting contribution to existing
knowledge.

TECHNICAL NOTES: Information less broad
in scope but nevertheless of importance as a
contribution to existing knowledge.

TECHNICAL MEMORANDUMS:
Information receiving limited distribution
because of preliminary data, security classifica-
tion, or other reasons.

CONTRACTOR REPORTS: Scientific and
technical information generated under a NASA
contract or grant and considered an important
contribution to existing knowledge.

TECHNICAL TRANSLATIONS: Information
published in a foreign language considered
to merit NASA distribution in English.

SPECIAL PUBLICATIONS: Information
derived from or of value to NASA activities.
Publications include conference proceedings,
monographs, data compilations, handbooks,
sourcebooks, and special bibliographies.

TECHNOLOGY UTILIZATION
PUBLICATIONS: Information on technology
used by NASA that may be of particular
interest in commercial and other non-aerospace
applications. Publications include Tech Briefs,
Technology Utilization Reports and
Technology Surveys.

Details on the availability of these publications may be obtained from:

SCIENTIFIC AND TECHNICAL INFORMATION OFFICE

NATIONAL AERONAUTICS AND SPACE ADMINISTRATION
Washington, D.C. 20546